Geomorphology
July 2022, Volume 408 Pages 108211 (16p.)
https://doi.org/10.1016/j.geomorph.2022.108211
https://archimer.ifremer.fr/doc/00803/91512/

Experimental field study on the fatigue and failure mechanisms of coastal chalk cliffs: Implementation of a multi-parameter monitoring system (Sainte-Marguerite-sur-Mer, France)

Letortu Pauline [1, *], Le Dantec Nicolas [2, 3, 4], Augereau Emmanuel [1, 3, 5], Costa Stephane [5], Maquaire Olivier [5], Davidson Robert [5], Fauchard Cyrille [5, 6], Antoine Raphael [6], Flahaut Reynald [7], Guirriec Yan [7], Longuevergne Laurent [8], De La Bernardie Jerome [8], David Laurence [9]

[1] Univ Brest, CNRS, LETG, IUEM, F-29280 Plouzané, France
[2] Cerema, Direction Eau Mer et Fleuves, 60270 Margny-lès-Compiègne, France
[3] Univ Brest, CNRS, Geo-Ocean, IUEM, F-29280 Plouzané, France
[4] Univ Brest, European Institute for Marine Studies (IUEM), CNRS, UMS 3113, F-29280 Plouzané, France
[5] Normandie Univ, UNICAEN, CNRS, IDEES, F-14000 Caen, France
[6] Cerema Normandie Centre, Research team ENDSUM, F-76121 Le Grand-Quevilly, France
[7] Cerema Normandie Centre, Regional Laboratory of Rouen, Earth Sciences group, F-76121 Le Grand-Quevilly, France
[8] University of Rennes 1, CNRS, Géosciences, F-35042 Rennes, France
[9] CNRS, LETG, IUEM, F-29280 Plouzané, France

* Corresponding author : Pauline Letortu, email address : pauline.letortu@univ-brest.fr

nicolas.ledantec@univ-brest.fr ; emmanuel.augereau@univ-brest.fr ; stephane.costa@unicaen.fr ; olivier.maquaire@unicaen.fr ; robert.davidson@unicaen.fr ; cyrille.fauchard@cerema.fr ; raphael.antoine@cerema.fr ; reynald.flahaut@cerema.fr ; yan.guirriec@cerema.fr ; laurent.longuevergne@uni-rennels1.fr ; jerome.delabernardie@univ-rennes1.fr ; laurence.david@univ-brest.fr

Abstract :

Between November 2018 and January 2020, a continuous multi-parameter survey, using nine types of sensors, was carried out on a coastal chalk cliff in Sainte-Marguerite-sur-Mer (Normandy, France) with the objective of gaining a deeper understanding of the forcing agents and processes that lead to cliff fatigue and failure. This paper will present the survey instrumentation, the results on the internal characteristics of the chalk massif, initial results (from November 2018 to March 2019) of the thermal subsurface behaviour along the cliff face, and the analyses of the observed cliff-top ground motion and the movement of existing fractures on the cliff face in relation to forcing agents. Our main results show that 1) the magnitude of cliff-top displacement on this coastal chalk cliff is consistent with prior studies conducted in different settings showing rather high displacement amplitudes (up to 50 mu m in relatively

calm conditions) likely to be related to chalk elasticity; 2) the displacement on existing fractures is partly controlled by the tidal amplitude, with a threshold response, but not only. Statistical analyses help the identification of other controls. The processing of the entire dataset from November 2018 to January 2020 with a combined analysis of multiple sensors' output is expected to provide further insight on cliff fatigue and failure.

Highlights

► A monitoring system was implemented along the cliff coast to better understand the agents that lead to fatigue and failure. ► For 13 months, 9 types of sensors recorded cliff mechanical response, marine agents and subaerial agents. ► Cliff-top displacements on this coastal chalk cliff showed rather high amplitudes, likely to be related to chalk elasticity. ► The displacement on existing fractures on the cliff face was partly controlled by the tidal amplitude but was multifactorial.

Keywords : Cliff erosion, Rock fall triggering mechanisms, Continuous monitoring, Instrumentation, Normandy

1. Introduction

Recent research on the evolution of rocky coasts, in particular the studies using environmental seismology, has led to an improved but incomplete understanding of cliff fatigue and cliff failure mechanisms (for a review, see Kennedy et al., 2014). Predicting when and where cliff failure will take place is difficult, but the stakes are high with the ever-increasing attractiveness of coastal areas (leading to population growth) (Balk et al., 2009), and climate change-related environmental changes that may contribute to the heightened vulnerability of coastal cliffs (IPCC, 2021, 2022). In such a context, natural hazards planning has become an essential component in the coastal management toolkit to help coastal communities, infrastructure, historical sites and economic sectors (tourism, fishing, leisure) to face up to these threats.

Cliff failure results from the interaction of both internal (e.g., rock strength, tectonics) and external factors. In coastal cliff environments, these external factors can include subaerial – including subsurface – agents (e.g., precipitation (Duperret et al., 2002; Brooks et al., 2012; Bernatchez et al., 2021; Young et al., 2021), water table fluctuations (Hutchinson, 1969; Lageat et al., 2006; Pierre and Lahousse, 2006), variations in temperature (Bernatchez et al., 2011, 2021; Letortu et al., 2015a)), marine actions (e.g., mean sea-level variations, tide, sea state (Guilcher, 1954; Robinson, 1977; Sunamura, 1977; Carter and Guy, 1988)) and anthropogenic phenomena (e.g., coastal defence structures that modify sediment transport (Costa et al., 2004)). In other environments, such as glacial and mountain regions, monitoring projects have identified the influence of rainfall (e.g., Rapp, 1960; André, 1997; Ilinca, 2009; Zielonka and Wrońska-Wałach, 2019; Mainieri et al., 2020), snowmelt (Reid et al., 1988), freeze-thaw cycles (e.g. Wieczorek and Jäger, 1996; Matsuoka and Sakai, 1999; Ilinca, 2009) and solar heating (Collins and Stock, 2016), to be the main triggering mechanisms for rock fall activity.

More often than not, major erosion factors are identified at specific coastal sites across the world (for a review, see Prémaillon et al., 2018). However, only a few studies have compiled

databases combining precise records of coastal cliff failure events and the associated forcing factors (e.g., Bernatchez et al., 2011; Letortu et al., 2015a; Young et al., 2021) enabling the contribution of erosion processes to be assessed. Since 2000, several studies have focused on wave-generated coastal cliff-top ground motions using broadband seismometers (Adams et al., 2002, 2005; Young et al. 2011, 2012, 2013, 2016; Dickson and Pentney, 2012; Norman et al., 2013; Earlie et al., 2015; Vann Jones (née Norman) et al., 2015; Kennedy et al., 2018; Laute et al., 2018; Vann Jones et al., 2018; Thompson et al., 2019). Although current understanding of wave-cliff coupling is by no means complete, cliff-top ground motions have been linked with specific marine processes believed to bring about these ground motions, and four frequency bands have been distinguished (limits slightly vary from one site to another): (1) Infragravity waves (IG) (0.005–0.05 Hz) which are mainly derived from swell (Bertin et al., 2018). It has been reported that the loading of the shore platform by IG waves causes a slow swaying motion at the cliff top (e.g., Adams et al., 2005; Young et al., 2011); (2) Swell, i.e., typical surface gravity waves (SF) (0.05–0.1 Hz), which also contributes to cliff-top swaying motions, at frequencies higher than IG (Young et al., 2011, 2013); (3) Double frequency (DF) (0.1–0.3 Hz), which corresponds to standing waves generated by wave/wave interactions; (4) High frequency (HF) (> 1 Hz), which is generated by a combination of local phenomena such as the direct impact of waves on the cliff face (Adams et al., 2002; Lim et al., 2011) or on the shore platform (Dickson and Pentney, 2012; Poppeliers and Mallinson, 2015), wind buffeting (Norman et al., 2013) and parasitic waves, mostly from anthropogenic sources. Cliff-top ground motions are good proxies for environmental forcing (Norman et al., 2013) and wave impact forcing using individual wave field measurements (Thompson et al., 2019), however, questions remain on the transfer function between wave action and cliff response, the spatial representativeness of the recorded ground displacement measurements, and the implication of these cliff-top micro-movements in terms of cliff failure.

There is a knowledge gap about how much each triggering factor contributes to cliff failure (Lim et al., 2010; Naylor et al., 2010; Kennedy et al., 2014), which is difficult to overcome as

unpicking the multifactorial elements involved to identify each dominant factors' contribution is an intricate process. The difficulty of this task stems from:

1) Difficulties in measuring failure events and underlying processes with sufficient temporal resolution (Lawler, 2005; Lim et al., 2010; Bernatchez et al., 2011);

2) Variable time lag between the forcing signature and the failure event, thus complicating the identification of correlations and highlighting the need for long-term monitoring (Viles, 2013);

3) Presence of a structural context and marine weather conditions that are often site-specific, and a time variable (including both meteorological variability and climate change) thus making it difficult to transpose results (Lee, 2008).

In order to overcome the first two above-mentioned scientific barriers, an ambitious, multi-parameter and continuous monitoring survey (13 months, from November 2018 to January 2020) was implemented at a chalk cliff site in Sainte-Marguerite-sur-Mer (Normandy, France), based on prior field monitoring experiments carried out in Brittany (Letortu et al., 2017; Laute et al., 2018). This work in Normandy is part of the RICOCHET project (2017–2021, http://anr-ricochet.unicaen.fr/), funded by the French National Research Agency (ANR). The parameters that were selected for monitoring were the key environmental ones evoked in the literature – cliff face/cliff top/cliff foot (temperature, precipitation, wind, tide, waves, etc.), internal (water table, temperature), and cliff behaviour (cliff-top ground motion, fracturing, deformation, possible failure events). Using a dataset that combined a precise record of cliff behaviour and the internal and external factors at very high temporal and spatial resolutions, the objective was to determine the contribution of different factors and processes in cliff evolution in Sainte-Marguerite-sur-Mer. It is expected that our study will provide insight to support model development for better forecasting of cliff failure/retreat, which in turn will help to address coastal management issues related to land planning in response to cliff erosion risks.

This first paper on this dataset has two objectives: (1) to describe the innovative instrumentation and the dataset (from November 2018 to January 2020), (2) to present the

results on the geophysical properties of the studied chalk site, and the initial results (from November 2018 to March 2019) on the subsurface thermal behaviour along the cliff face, the cliff-top ground motion observed, and the evolution of the existing fractures on the cliff face (opening or closure) in relation to external forcing factors.

2. Study area

2.1. Regional setting

The coastal cliffs of Sainte-Marguerite-sur-Mer are around 10 to 25 m high and located along the French side of the Channel in Seine-Maritime (Normandy, NW France). Tidal range is 8 m (macrotidal environment). The configuration of the Channel means that swell is limited along this coast: significant swell height $H_{1/3}$ is less than 2 m for 95% of the time and greater than 3 m for 0.3% of the time, i.e. about 25 h y^{-1} (Teisson, 1986). However, wind wave height may be high with a maximum significant wave height of 4.3 m in Dieppe (one-year return period) (Augris et al., 2004). Geologically, the “Pays de Caux” plateau terminates at the coastline in cliffs made up of Upper Cretaceous chalk interbedded with flint bands (Pomerol et al., 1987; Mortimore and Duperret, 2004). There are some subtle contrasts in rock strength in the different stages of chalk: in some areas, the residual flint formation over these chalk strata (Laignel, 1997; Costa et al., 2006b) has been replaced by a bed of clay and sandy sediments of around 10–30 m thick from the Paleogene age (Bignot, 1962), which is particularly present in Sainte-Marguerite-sur-Mer, Varengeville-sur-Mer and Sotteville-sur-Mer where the cliff lithology is rather complex (Figure 1). Erosion dynamics are spatially variable (from 0.09 m y^{-1} to 0.23 m y^{-1} (1966–2008), Letortu et al., 2014a) mainly due to lithologic control (Costa, 1997; Costa et al., 2004, 2019). There is an erosion hotspot along the Cap d’Ailly where a rock fall (used to describe movements of coherent rock, consistent with Varnes, 1978) from 1 000 m^3 has a return period of six months per linear kilometre and retreat rates can locally exceed 0.80 m y^{-1} (Letortu et al., 2014a).

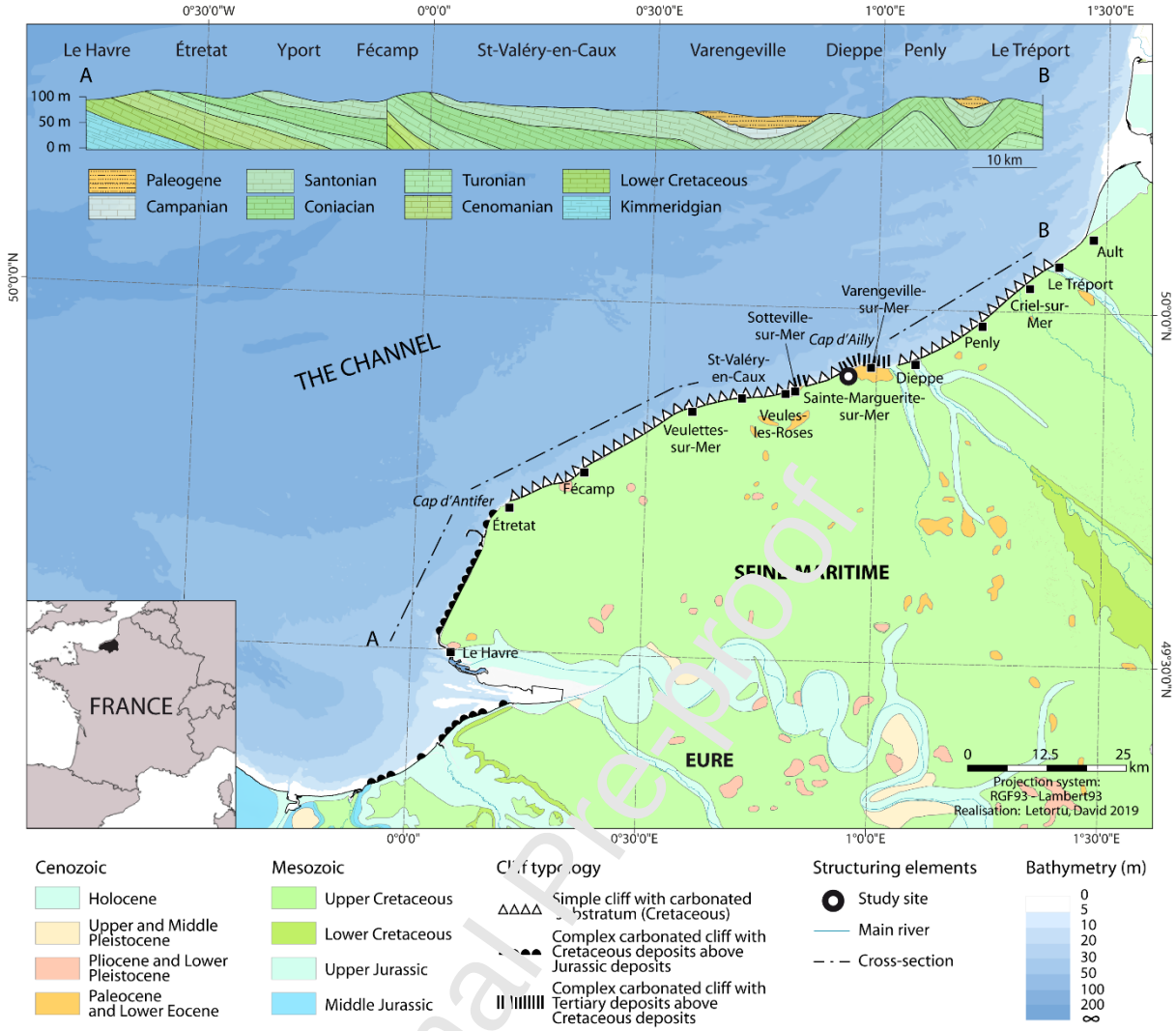

Figure 1: Geology in Normandy, cliff typology and location of the study site in Sainte-Marguerite-sur-Mer.

The cliff foot is characterised by a rocky platform and a gravel barrier in the upper beach against the cliff. The platform is wide (from 100 m to 750 m) with a homogeneous slope (from 0.2% at Le Tréport to 2% at Cap d'Antifer). The gravel barrier is on average about 15–20 m wide, and 2–3 m thick. Beach thickness and width are highly variable along the coast, especially where cross-shore sea defence structures (jetties, groynes) have been constructed, near the stakes (at the valley outlets, as in Sainte-Marguerite-sur-Mer (Figure 2a)). There, the gravel beaches can be more than 100 m wide and up to 11 m thick at the Dieppe jetty (Costa et al., 2006a).

The Seine-Maritime coast has an oceanic temperate climate. Mean winter temperatures are positive (5.2°C in January and February) with an average of 30 frost days recorded each year (minimal temperature can reach -16.6°C in February). Precipitation occurs throughout the year (798.2 mm), with autumn and summer being the wettest seasons (minimum of 51.5 mm in February, and maximum of 89.8 mm in October). Daily rainfall can reach 100.8 mm in August. Winds are frequent and violent with an average wind speed of 5.1 m s^{-1}, especially from November to February (66% of the average number of days with gusts over 16 m s^{-1}), with a dominant westerly direction (southwest to northwest) (Dieppe station (1981–2010), Météo-France, 2019).

2.2. Study site selection and characteristics

The chalk cliff site of Sainte-Marguerite-sur-Mer (N 49°54'34'', E 0°56'18'', NW orientation) was selected for our 13-month field measurement survey (November 2018–January 2020) for the following reasons:

- It is located in the Cap d'Ailly erosion hotspot (Costa et al., 2004, 2019; Letortu et al., 2014a, 2014b) where the cliff line has been increasingly monitored to gain more knowledge about erosion (e.g., Prêcheur, 1960; Evrard and Sinelle, 1987; Costa et al., 2004, 2019; Mortimore et al., 2004; Letortu et al., 2015b, 2019). There is a general consensus that the main drivers of erosion are lithological control (Costa et al., 2004), intense rainfall events (Duperret et al., 2004; Lageat et al., 2006; Letortu et al., 2015b) and marine factors (Letortu et al., 2015a, 2015b, 2019);
- The cliff foot is accessible via the nearby Sainte-Marguerite-sur-Mer beach (at the outlet of the Saâne River), the cliff top via a nearby parking facility, and through a farmed field using a motorised, off-road vehicle, there is also a hiking path;
- Legal authorizations to carry out the monitoring were obtained (local authority, the plot's owner and farmer).

The monitoring survey focused on a 225 m-long cliff section located downdrift of a groyne (which had caused the formation of a lookout point by differential erosion) and a former

bunker (which has now fallen on the platform), both of which have affected the alongshore beach and cliff morphology (Figure 2a). Topographic surveys of the cliff were carried out by Terrestrial Laser Scanning (TLS) from the last groyne to 100 m downdrift of the bunker, where the cliff height is around 20 m (measured above the gravel barrier at the cliff foot).

The chalk of the cliff face is particularly weathered (from chemical, biological and mechanical processes which have led to rock fracturing and failure) at this site (grade 3 to 4 on the "weathered rock state" scale of the International Society of Rock Mechanics (ISRM) (WSDOT, 2021)) showing a dense network on small factures on the surface with 10 to 30 cm spacing ("closely spaced" on the "discontinuity spacing" scale on the ISRM (WSDOT, 2021)). The different instruments were set up on the cliff face and cliff top near the central part of this 225 m-long cliff section, in an area where the chalk on the cliff face was not too weathered (for safety purposes during the installation). As the instrumented site is downdrift of the groynes on the beach, the gravel beach at the cliff foot is narrow (about 30 m compared to 80 m at the last groyne) with a height difference of around 4 m (Figure 2a).

The topography of the site on the cliff top is particular and has a significant impact on the characteristics of the water table at this site. The large-scale seaward slope of the plateau shows an inversion near the coast on the landward slope. In addition, this is a gentler, SW alongshore slope. This topography is associated with a drainage system that is oriented parallel to the cliff edge, including a small intermittent stream located around 60 m from the cliff edge (Figure 2a).

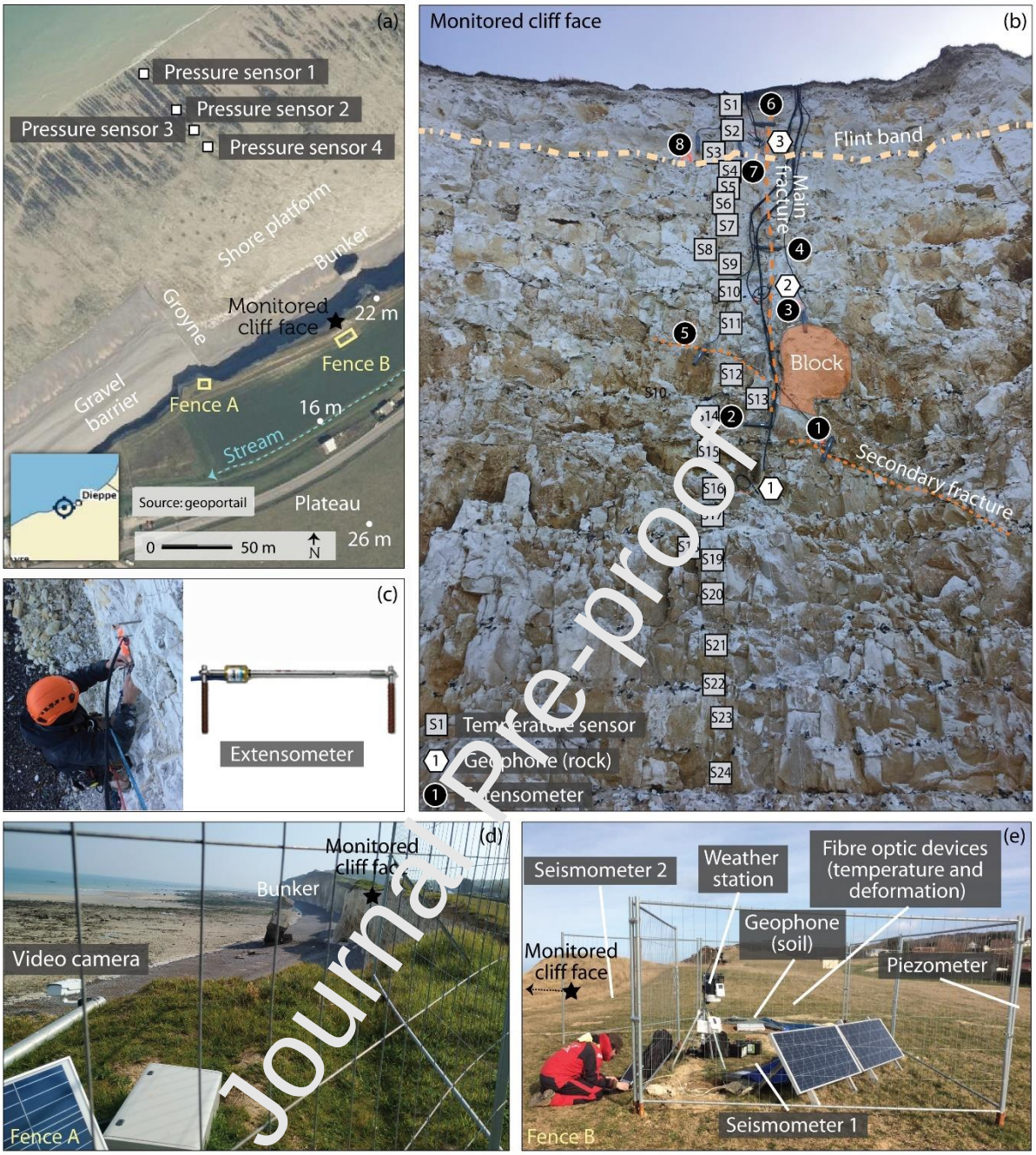

Figure 2: (a) Location of the sensors on the cliff top and the shore platform, and some structuring elements of the Sainte-Marguerite-sur-Mer site; (b) monitored cliff face (view from the gravel barrier), also showing the visual aspect of the chalk on the cliff face; (c) extensometer and set-up on the cliff face; (d) sensors located in fence A at the cliff top; (e) sensors located in fence B and vicinity, at the cliff top.

3. Field monitoring methods

The instrumentation comprised 44 sensors of 9 different types that were set up on the cliff top, cliff face and shore platform to record the following (Figure 2, Table 1):

- Cliff mechanical response (seismometers, geophones, extensometers, fibre optic);
- Marine forcing (pressure sensors, video camera);
- Subaerial forcing (weather station, temperature sensors, fibre optic, piezometer).

Most of the instruments used were commercially available, and had undergone some modification for this particular use. All instruments were deployed within the same cross-shore plane, comprising the vertical cliff profile and intertidal cross-shore profile (Figure 2a). The video acquisition system was deployed on a lookout point (Figure 2a), at a distance of around 105 m from the instruments' location, which enabled the cliff face, from the lookout to the bunker, and the upper beach to be monitored (Figure 2d).

Table 1: List of sensors deployed and their characteristics at the Sainte-Marguerite-sur-Mer site

Survey	Sensor	Quantity	Location	Duration	Sampling frequency	Sensor detail
Cliff mechanical response	Seismometer	1	Cliff top	November 2018-January 2020	100 Hz	Trillium Compact Posthole (Nanometrics), 0.0083-100 Hz
	Seismometer	1	Cliff top	October 2019-January 2020	200 Hz	NoeMax (Agecodagis) 0.033-200 Hz
	Geophone (soil)	1	Cliff top	November 2018-January 2020	4.5-100 Hz, event-trigerred	Triaxial (IMS)
	Geophone (rock)	3	Cliff face	November 2018-January 2020	4.5-100 Hz, event-trigerred	Triaxial (IMS)
	Extensometer	8	Cliff face	November 2018-January 2020	30 min	4420 VW (Geokon)
	Fibre optic device for defomation measurements	1	Cliff top borehole	November 2018-January 2020	20 s	Two measurement sessions of 12 h, spatial resolution of 2 cm

Marine forcing	Pressure sensor	4	Shore platform	November 2018-January 2020	5 Hz	Wave gauge (OSSI)
	Video camera	1	Nearby lookout on the cliff top	November 2018-January 2020	30 min h^{-1} in daytime	Camera P-1365-E (Axis)
Subaerial forcing	Weather station (including 2 soil moisture sensors)	1	Cliff top	November 2018-January 2020	2 h	Vantage Pro 2 (Davis)
	Temperature sensor	24	Cliff face	November 2018-January 2020	1 h	Flying Lead Thermistor Probe (Tinytag)
	Fibre optic device for temperature measurements	1	Cliff top borehole	November 2018-January 2020	1 min	Two measurement sessions of 12 h, spatial resolution of 25 cm
	Piezometer	1	Cliff top	November 2018-January 2020	1 h	CNR10R (Panatronic)

3.1. Cliff mechanical response

The cliff-top ground motions were recorded by a broadband seismometer (0.0083–100 Hz) located at the cliff top (17 m from the cliff edge), buried about 0.5 m in the soil. Near the end of the monitoring period, in October 2019, a second seismometer (0.05–100 Hz) was installed between the cliff edge and the seismometer 1 (Figure 2e), to (1) examine cliff deformation as opposed to displacement, (2) enable sources of seismic signals to be localized, and (3) assess the cliff's material properties with respect to the propagation of seismic signals.

Cliff micro-fracturing was monitored with four geophones: three were setup in horizontal boreholes on the cliff face in subsurface (0.7 m deep in the chalk) at different heights to measure micro-fracturing evolution in space (at heights of 7 m, 10 m and 14 m in IGN69 (official vertical datum in France), respectively and vertically aligned (noting that the cliff foot is at 1.6 m high in IGN69)) (Figure 2b). A vertical geophone (soil geophone) was installed at the cliff top near seismometer 1, and buried 1 m deep in the soil (Figure 2e). Near the vertical array of the three cliff-face geophones, the evolution of a number of existing fractures on the

cliff surface was monitored using eight extensometers (installed at the location from 7 m to 15 m high in IGN69) (Figure 2b and 2c). The sensors used had a +/- 12.5 mm extension range. Extensometers 4 and 6 were located on the main oblique fracture identified on the cliff face, and 1 and 5 were each located on a secondary fracture. Extensometer 3 was positioned over a well-identified block, 7 across a flint band and 8 above the previous flint band. Extensometer 2 was placed on a solid piece of chalk. The idea behind this set-up is to examine whether and how displacements recorded at the cliff top cause micro-fracturing and eventually cliff failure, and to investigate the evolution and role of existing fractures on the face in the cliff's mechanical response.

Distributed deformation measurements were also collected over two continuous sessions of about 12 h with a fibre optic device, allowing a spatial resolution of 2 cm along the fibre optic cable at 20 s temporal resolution (Figure 2e, Table 1). The objective was to investigate the cliff's mechanical response along its full height as opposed to only at the cliff top. The depth-dependence of the deformation, induced by the combination of marine and subaerial forcing factors, may make it possible to identify potential zones of maximum deformation at certain heights along the cliff, depending on its geometry, lithology and hydrology. The cable was cemented in a vertical borehole located near the seismometer, 18 m from the cliff edge, in a 2-way configuration running from the cliff top to the cliff foot and back (Figure 2e). The two data acquisition sessions occurred during spring tides, in the spring and autumn of 2019.

3.2. Marine forcing

To monitor hydrodynamic conditions, pressure sensors located on the shore platform were used to measure wave parameters and water level, along with a video camera to assess the sea-surface conditions and characterise the impact of the waves on the cliff face.

Four pressure sensors were set up along a cross-shore transect in the same plane as the vertical array of instruments on the cliff face (Figure 2a). They were located on the lower to middle sections of the intertidal zone to ensure sufficient immersion time at water depths beyond the surf zone at each tidal cycle (at a distance of between 158 m and 233 m from the

cliff). These four sensors were deployed to account for possible instrument failure (only three are needed), given the importance of this forcing agent and the duration of the field survey, and to also provide insight on wave transformation across the shore platform.

A video acquisition system positioned on a lookout at the cliff top (Figure 2d) provided qualitative observations on the sea-surface conditions in the upper beach and at the foot of the cliff, as well as on individual wave impacts on the gravel barrier and on the cliff when they occur. Wave impacts can be identified individually, together with a characterisation of wave-breaking type and a wave-by-wave assessment of water levels against the cliff. The video camera was also used to monitor the morphological evolution of the cliff and beach, the occurrence of failure events, and provide a precise timing of the event. Video recording of the upper beach also provided quantitative information on the evolution of the gravel barrier morphology by calibrating the images from the camera and using water level measurements from the pressure sensors to obtain the elevation of the water line on time-stacked images. Through the combined measurements of the cliff's mechanical response, data on hydrodynamics forcing and the beach and cliff morphological evolution, meant that wave-cliff-beach interactions could be examined.

3.3. Subaerial forcing

The monitoring focused on three main factors: rainfall, groundwater level within the chalk cliff, and temperature variations of the cliff face and the chalk massif. A weather station deployed at the cliff top near the seismometer 1 and soil geophone, located 17 m from the cliff edge, recorded rainfall, wind speed and direction, air temperature, and soil moisture (Figure 2e). A piezometer was installed in a 30 m deep borehole located on the cliff top, 38 m from the instrumented cliff face (Figure 2e). The subsurface temperature of the cliff face was measured every 30 minutes using an array of 24 temperature sensors embedded 15 cm deep into the cliff (away from fractures) along a vertical profile from 50 cm under the top of the cliff face (21 m IGN69) to the bottom of the cliff face (9.5 m IGN69), spaced at 50 cm intervals (Figure 2b).

This set-up aims to provide insight on the role of hydrological processes (including run-off, infiltration, groundwater pressure build-up) on cliff fracturing and failure. Rainfall events are known to contribute to cliff retreat, sometimes acting as triggers, with variable time lags between the rainfall event and the cliff failure. The contributions from the various rainfall-induced mechanisms are still unclear. On our study site, due to the specific topographic configuration, the water table within the cliff is under the influence of both local effects with short response time (discharge of the adjacent stream, tidal level) and regional-scale fluctuations in the groundwater level. Groundwater level can also be used as an input to evaluate the contribution of pore pressure to the total stress exerted on the cliff.

Another contributing factor to cliff retreat is thermal fluctuations. Subsurface temperature monitoring will enable the examination of short-term sunlight-related temperature fluctuations within the chalk, and sea surface conditions and tide, including sea spray effects. Due to the spatial distribution of the temperature sensors, height-dependent processes along the cliff face can be investigated, such as the effects of solar radiation gradients between the cliff top and foot and the propagation of thermal fronts related to rainfall infiltration and groundwater level fluctuations.

A second fibre optic device was used to collect distributed temperature measurements in the chalk massif, with a 25 cm spatial resolution along the cable and 1 min temporal resolution, during the same two sessions of around 12 h as the distributed deformation measurements (Figure 2e, Table 1). The cable was deployed in the same borehole and with a similar two-way configuration as the cable for deformation measurements. The borehole temperature data will complement the subsurface temperature measurements recorded on the cliff face throughout the entire monitoring period. In particular, we will be able to distinguish superficial thermal processes occurring on the cliff face from processes affecting the whole cliff formation, and also establish a stronger link between hydrology and deformation (assuming that temperature gradients along the borehole are linked to groundwater circulation and indicative of variations in the mechanical properties of chalk).

3.4. Complementary data: topographic and thermal surveys of the cliff face and geophysical site characterisation

In addition to the continuous, multi-parameter monitoring, complementary data were acquired before and during the instrumentation period (Table 2): thirteen topographic surveys (every three months, except in the autumn and winter of the 2018–2019 period where survey periodicity was monthly) were performed to quantify the precise morphological evolution of the cliff face, six surveys of the surface temperature of the cliff face section (125 m-long, every three months from November 2018 to May 2019) to complement the localised subsurface temperature monitoring, and a geophysical survey to characterise the subsurface ground properties at the site under study.

Repeated topographic surveys of the monitored cliff face were carried out from the shore platform by TLS following the protocol used in Letortu et al. (2019). These began in November 2017, with temporal frequency of about 3 months, 225 m-long, on both sides of the monitored cliff face (Table 2a). Eight surveys were performed during the monitoring period, including two surveys immediately before and after installing the instrumentation, and two surveys before and after removing the instrumentation to quantify the potential anthropogenic erosion (Table 2b).

Surface temperature data of the cliff face were collected from the beach using an infrared camera (FLIR T650sc 45°), coupled with a regular camera so that the mosaic of temperature photographs can be draped over the cliff photograph. While subsurface monitoring with the different sensors is supposed to monitor temperature at different timescales from sub-daily to seasonal, the surface temperature surveys are supposed to identify potential spatial differences in the thermal behaviour of the cliff face depending on its properties (chalk colour, flint bands, etc.). Four surveys were carried out during the monitoring period (Table 2b).

A geophysical survey, coupling Ground Penetrating Radar (GPR) and Electrical Resistivity Tomography (ERT) measurements (with a Terrameter LS 2 (ABEM)), was performed in March 2018 (Table 2a) to assess the chalk homogeneity at this site and to provide some information on its internal structure and properties (methodology described in Fauchard et

al., 2013). The survey consisted of a profile on the cliff top along the cliff edge and two cross profiles running in a cross-shore direction from the cliff top to the gravel barrier on the beach and including the cliff face (Figure 5a). The longitudinal ERT profile was carried out on the cliff top, alongside the cliff edge, 10 m from the main scarp, using a 256 m-long Wenner array composed of 128 electrodes at 2 m intervals. A 256 m-long GPR profile was realised along the same transect with a 200 MHz dipole antenna. The first seismometer (fence B in Figure 2e) was located at 102 m (from the NE extremity) along the geophysical measurements profile.

Table 2: Timeline of the surveys performed (a) before and (b) during the multi-parameter monitoring (TLS: Terrestrial Laser Scanning).

(a) Before monitoring	Nov-17	Dec-17	Jan-18	Feb-18	Mar-18	Apr-18	May-18	Jun-18	Jul-18	Aug-18	Sep-18	Oct-18
TLS survey [number of surveys]	[1]			[1]	[1]				[1]			[1]
Cliff face thermal survey [number of surveys]	[2]											
Geophysical survey [number of surveys]					[1]							

(b) During	Nov-	Dec-	Jan-19	Feb-	Mar-	Apr-	May-	Jun-	Jul-	Aug-	Sep-	Oct-	Nov-	Dec-	Jan-20

monitoring	18	18		19	19	19	19	19	19	19	19	19	19	19	
TLS survey [number of surveys]	[2]	[1]	[1]					[1]			[1]				[2]
Cliff face thermal survey [number of surveys]	[1]			[1]			[1]								[1]
Fibre optic survey (temperature) [duration]							[12 h]						[12 h]		
Fibre optic survey (deformation) [duration]							[12 h]						[12 h]		

4. Data analysis methods

4.1. Geophysical site characterisation

According to the methodology described in Fauchard et al. (2013), ERT measurements were inverted using Res2Dinv software (Loke, 2002, 2004). The number of iterations and root mean square were 7 and 0.22%, respectively. These two values ensure the best fit between the calculated model and the measured resistivities in the least-square sense. GPR measurements were performed with a SIR 3000 and a bowtie antenna (GSSI) and the

measurements were processed with the Reflex software (Sandmeier Geophysical Research, 2019) using a standard processing chain (including background removal, Butterworth band pass filter and adjusted gain for improved visualisation).

4.2. Cliff-top ground motion measured by broadband seismometer

Data from the seismometer 1 deployed throughout the entire field campaign (broadband, 120 s-100 Hz) is briefly presented here. Only the vertical component of the seismometer's signal is considered, as horizontal components tend to be significantly affected by ground tilt (Rodgers, 1968). The processing steps consisted in:

1) Deconvolution of the instrumental response;

2) Bandpass filtering (Butterworth), with cut-off frequencies at 0.0083 and 50 Hz, as defined by the manufacturer;

3) Data clean-up, to discard periods with anthropogenic activities and remove transient signals following instrument restart after a power loss;

4) Integration of the velocity response into displacement using the trapezoidal method;

5) Computation of the spectrum (Power Spectral Density, PSD) and spectrograms (computed using 20 min windows with 90% overlap) of vertical displacement.

Figure 3 shows an example of PSD of vertical displacement for a selected day (13 November 2018), typical of mildly energetic hydrodynamic conditions. We verified that energy levels in the DF band were consistent between our cliff-top seismometer and the inland reference station. We calculated the total displacement energy within each of the four frequency bands.

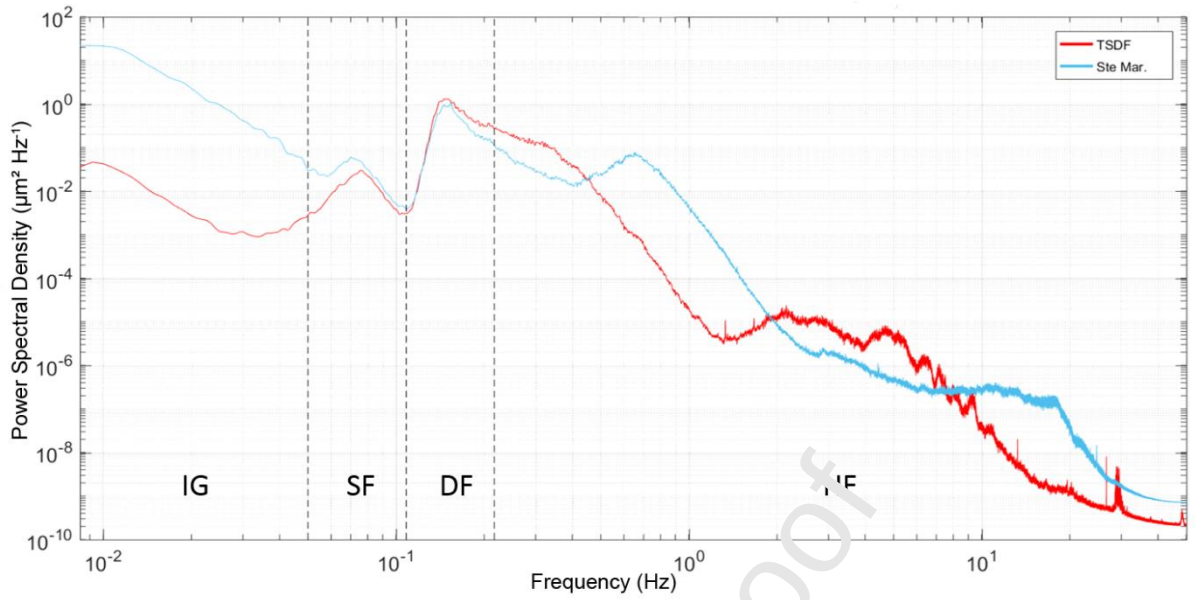

Figure 3: Power Spectral Density (PSD) of the displacement recorded by the seismometer on 13 November 2018, comparing between Sainte-Marguerite-sur-Mer station (Ste Mar.) and Thoiré-sur-Dinan (TSDF) inland station. The labels IG, SF, DF and HF indicate frequency bands, as explained in the text.

4.3. Displacement on existing cliff fractures measured by extensometers

We applied bivariate and multivariate statistical methods on our dataset. Because temporal sampling was different from one instrument to the other, we use the lowest temporal sampling (2 h, for the weather station) as our time scale. The data series of all the other instruments were resampled at two-hour intervals. The data of the eight extensometers were filtered using a 5 µm threshold for the range beyond which evolutions were considered as significant (values between -5 µm and 5 µm are considered as not significant) (Figure 4).

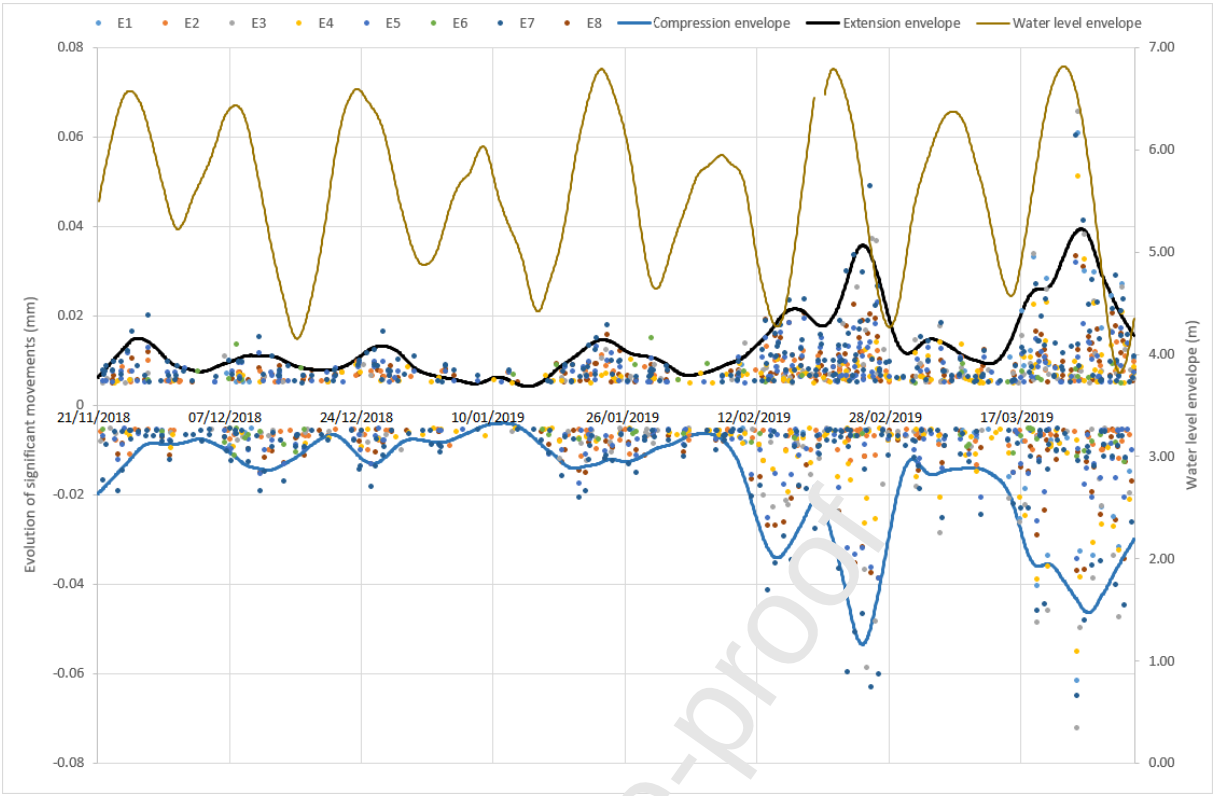

Figure 4: Extract of significant movement data from the eight extensometers (E, numbering from the middle (7 m IGN69) to the top of the cliff face (15 m IGN69) (Figure 2b)) from 21 November 2018 (00:00) to 31 March 2019 (22:00). The envelopes of the extension and the compression data considering all the extensometers are plotted in black and blue, respectively. The envelope of the water level data is plotted as well, to visualize the tidal cycles.

A selection was made among environmental factors in order to remove redundant data, which were identified with a correlation matrix calculated considering all factors (factors with Pearson's correlation above 0.65 were removed). Six synthetic environmental variables (subaerial and marine) were selected: sum of rainfall (mm) (sum over 2 hours), mean temperature (°C) (over 2 hours, mean of the upper 15 temperature sensors at the subsurface of the cliff face), wind speed (m s^{-1}), mean water level (m) (over 2 hours, observed tide and storm surge), maximum significant wave height (m) over 2 hours (largest value of the time series of significant wave height, calculated at a time step of 5 min) and tide coefficient.

Periods with data gaps on one of the variables (due to instrument failure) were removed, leaving an extensometer dataset from November 2018 to March 2019 consisting of 1229 individuals (two-hour periods with and without displacements): 576 showing significant displacements (active individuals) and 653 showing no displacements (supplementary individuals). The population of active individuals is large enough to perform statistical analyses. The data were standardised.

Analyses carried out using both populations made it possible to identify the environmental factors (subaerial, marine) that discriminate between two-hour periods with and without displacements, that is, identifying the conditions most prone to cause fracture movement, and whether certain factors induce a characteristic pattern of displacement (in intensity of occurrence). Analyses carried out on the population of active individuals only were meant to examine more precisely the displacements' characteristics (direction of displacement) as a function of the subaerial and marine conditions that were identified as conducive to fracture movement.

Details on the statistical analyses are presented in Table 3, where the dashed, vertical line is used as a separation to distinguish between the two aforementioned analyses. In both cases, we used multivariate (Principal Component Analysis, PCA; Hierarchical Cluster Analysis, HCA) and bivariate (χ^2 test) statistical methods, which were sequenced in four steps (Table 3):

1) A PCA was performed to visualise the links between variables and the existence of groups of individuals and groups of variables (Saporta, 2006). This structure highlights the agent(s) a priori most relevant to synthesise the subaerial and marine conditions that characterise individuals;

2) The second step was a HCA (Euclidean distance, Ward's method), for which we used the results of the PCA: the variables of individuals are their PCA coordinates on the first two axes. This step differentiates individuals (two-hour periods in the first analysis, or significant displacements in the second analysis) as a function of their associated subaerial and marine agents, leading to typologies of (a) subaerial and marine conditions causing significant

displacements, or not, and (b) significant displacements as a function of subaerial and marine conditions;

3) The third step consisted in an average analysis using these typologies, yielding the mean characteristics of subaerial and marine conditions leading to fracture movement, or not, or the mean environmental characteristics of significant displacements recorded on the cliff face. The characterisation of "low", “medium” or “high" is derived from the comparison of the mean (for the variables of interest) for the class with the overall mean (all individuals). For a given variable, the mean for a class is considered as "medium" if it is within plus or minus one standard deviation of the overall mean.

4) In the fourth step, complementary information on displacements was taken into consideration (intensity of displacements, frequency of occurrence of displacements and displacement direction). A χ^2 test (independence test, p-value between 0.3 to 7%) was performed to check whether certain types of subaerial and marine conditions preferentially generate displacements with a given intensity and with a given number of extensometers showing significant displacements. Furthermore, considering each measured displacement (every 30 min) instead of two-hour period, and associating displacements with their type, makes it possible to examine whether certain conditions trigger specific direction of displacements (closing or opening).

Methods	Displacement measurements recorded by extensometers	
1st step: PCA *Visualizes relationships between variables, presence of groups of individuals and groups of variables*	Subaerial and marine variables: sum of rainfall, mean temperature, wind speed, mean water level, maximum significant wave height, tide coefficient Active individuals: 2 h periods with displacements Supplementary individuals: 2 h periods without displacements	
2nd step: HCA *Differentiates subaerial and marine characteristics of 2 h periods or displacements and create a typology*	Individuals: Coordinates of 2 h periods on PCA factors	Individuals: Coordinates of 2 h periods on PCA factors Typology of PCA is integrated to displacements, which become individuals
3rd step: Average of clusters on factorial coordinates and variables *Characterises types of subaerial and marine conditions*	Individuals: 2 h periods with or without displacements Variables: same as 1st step	Individuals: Displacements Variables: same as 1st step
4th step: χ^2 test *Identifies the relationships between subaerial and marine condition types and displacement characteristics*	2 tests: - Types of subaerial and marine conditions/intensity of displacements in absolute value ((0; ≤0.01 mm; between but not including 0.01 and up to 0.03 mm; >0.03 mm) - Types of subaerial and marine conditions/ number of extensometers with displacements (0; 1-2; 3 and more)	1 test: - Types of subaerial and marine conditions/ displacement direction (contraction; extension)

Table 3: Analysis steps using multivariate and bivariate statistical methods, showing both analysis pipelines (separated by the dashed, vertical line)

5. Results

5.1. Internal structure and properties of the site

The longitudinal ERT profile clearly shows a two-layer structure (Figure 5c). The first layer, referred to as the upper chalk part, from the cliff top to the cliff foot (around 0 m IGN69), has resistivities ranging from 60 Ω m to over 300 Ω m, and averaging slightly above 100 Ω m. The second layer, from the cliff foot and extending at least 20 m beneath, shows much lower resistivity values (average of 4 Ω m). This information indicates that chalk is saturated with

highly conductive fluids in this underlying stratum, probably corresponding to seawater infiltrating all the cliff foot and mixing with inland groundwater.

The upper part of the chalk cliff is resistive enough to let electromagnetic waves propagate. The GPR depth of investigation is around 12 m (with an electromagnetic wave speed set at 1.3 m ns^{-1}, i.e. a dielectric constant of 5.3) and can be correlated with the resistivity pattern in the upper chalk layer. GPR signals between 60 and 200 m along the profile and down to a depth of 5 m reveal a heterogeneous chalk, probably resulting from open cracks filled with air and silt. Deeper (underneath the heterogeneous surface sub layer) and around this central area (at the extremities of the profile), radar signal strength has lower contrasts, indicating a homogeneous media compared with the wavelength (0.65 m) (Figure 5b).

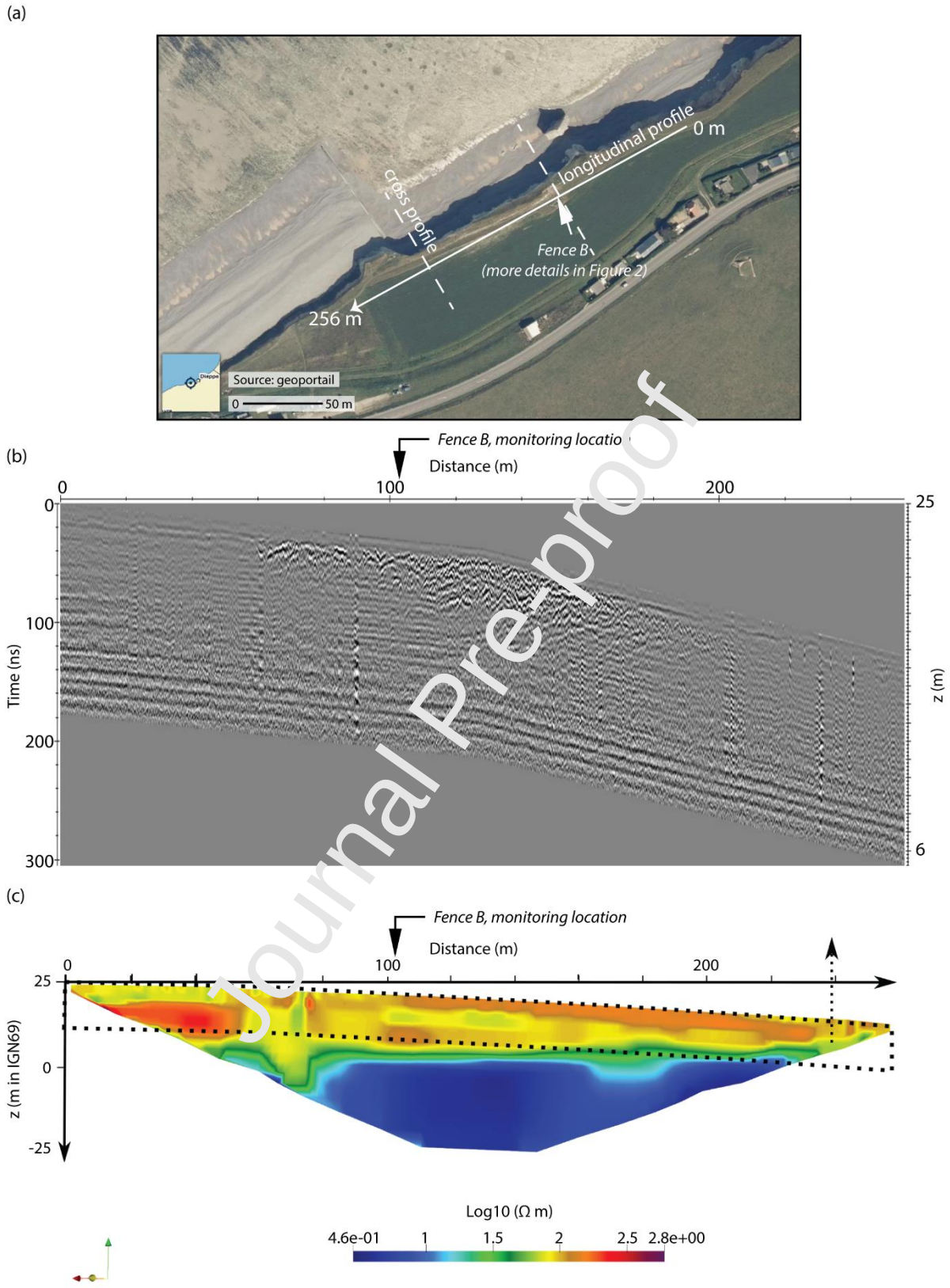

Figure 5: (a) Geophysical measurements location; (b) Ground Penetrating Radar (GPR) longitudinal profile (200 MHz, 12 m penetration depth); (c) Electrical Resistivity Tomography (ERT) longitudinal profile acquired on the cliff top, along the edge of the cliff, passing by

fence B (located in Figure 2). The common layer of investigated subsoil with GPR and ERT is delineated by the black dotted line. Note that the topography is enhanced in the GPR image; the depth scale differs compared with the ERT case.

5.2. Analysis period: is it representative of typical environmental conditions?

The analysis period (from November 2018 to March 2019) for the initial results of this unique dataset presented here was out of the ordinary in relation to typical forcing conditions. Autumn and winter were milder than the 30-year climatic normal (1981–2010) of Dieppe during these months. Minimal temperature was higher (+88%) than the climatic normal. We recorded 14 freeze days compared to 29 days for the climatic normal (from November to March), lower rainfall (-22%) and wind speed (-10%). Furthermore, there were no storms or major erosion events during this period (see TLS surveys in Figure 6), which is rare in winter. Only small rock falls (or flakes) of about 1 m³ were observed on the instrumented cliff face, mostly near the cliff foot.

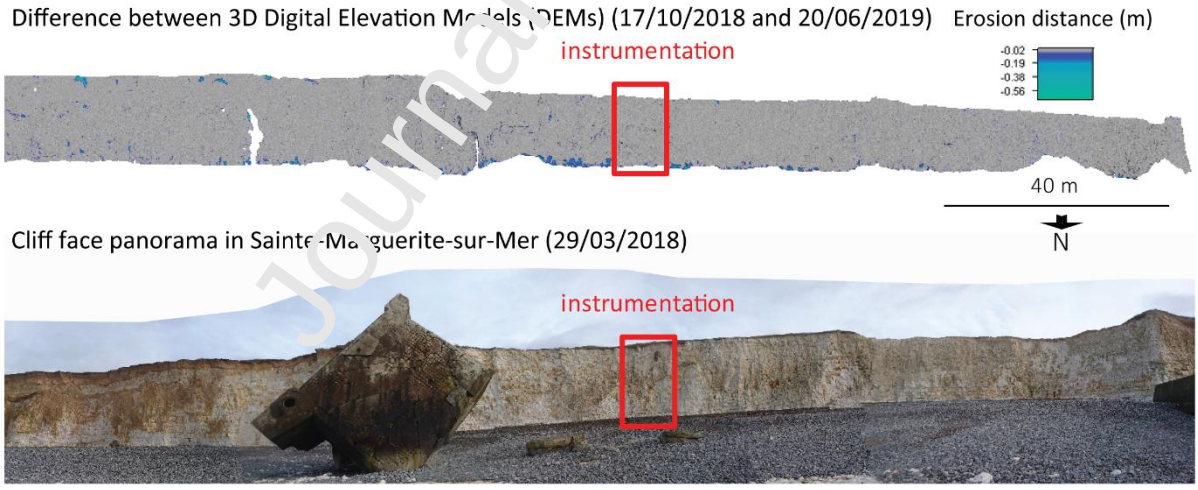

Figure 6: Cliff face erosion monitored by Terrestrial Laser Scanning (TLS) between 17/10/2018 and 20/06/2019 at Sainte-Marguerite-sur-Mer

5.3. Subsurface temperature variations along the cliff face

The subsurface temperature sensors array shows a good agreement with the weather station located on the cliff top (23.5 m IGN69). Higher frequency signals are present in the weather station records. The 24 h smoothing of weather station data shows a good fit with, for instance, sensors 3, 11, and 20 (20 m, 16 m and 11.5 m IGN69, respectively, Figure 2b) (Figure 7).

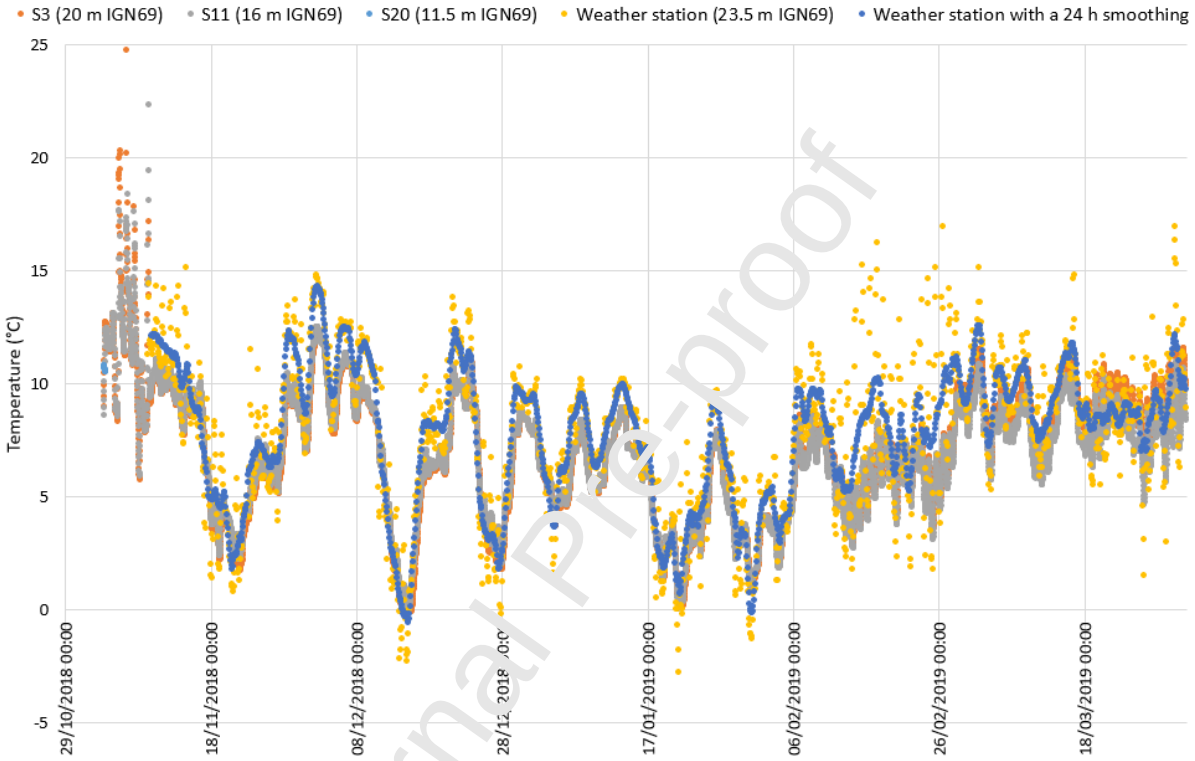

Figure 7: Temperature sensors at the subsurface of the cliff face from November 2018 to March 2019 (S3: sensor 3 located at 20 m IGN69, S11: sensor 11 located at 16 m IGN69, S20: sensor 20 located 11.5 m IGN69; weather station located on the plateau at 23.5 m IGN69 (Figure 2)).

Temperature gradients have been calculated for different time periods for sensors 3, 11 and 20. We observed a progressive increase of the short-term (over a few hours) temperature gradients of the 24 sensors as a function of the height along the cliff face (Figure 8), with slight discrepancies in the ordering of sensors due to the differences in depth of insertion into the cliff face and in the weathering of the chalk.

In the case of a decrease of external temperature over a week, from 8/12/2018 (21:00) to 15/12/2018 (05:00), the gradients of the subsurface sensors 3, 11 and 20 are -0.04°C per 30-min, -0.04°C per 30-min, -0.03°C per 30-min, respectively. In the case of a rapid decrease of external temperature over a night, from 24/12/2018 (18:30) to 25/12/2018 (09:30), the gradients of the subsurface sensor 3, 11 and 20 are -0.13°C per 30-min, -0.12°C per 30-min, -0.10°C per 30-min, respectively. In the case of an increase of external temperature over 3 days, from 15/12/2018 (17:00) to 17/12/2018 (15:30), the slopes of the subsurface sensors 3, 11 and 20 are 0.07°C per 30-min, 0.06°C per 30-min, 0.05°C per 30-min, respectively. In the case of an increase of external temperature over a day, 25/12/2018 (09:30–15:30), the slopes of the subsurface sensors 3, 11 and 20 are 0.06°C per 30-min, 0.11°C per 30-min, 0.00°C per 30-min, respectively. This behaviour highlights a decrease in thermal inertia from the top to the bottom of the cliff (Figure 8).

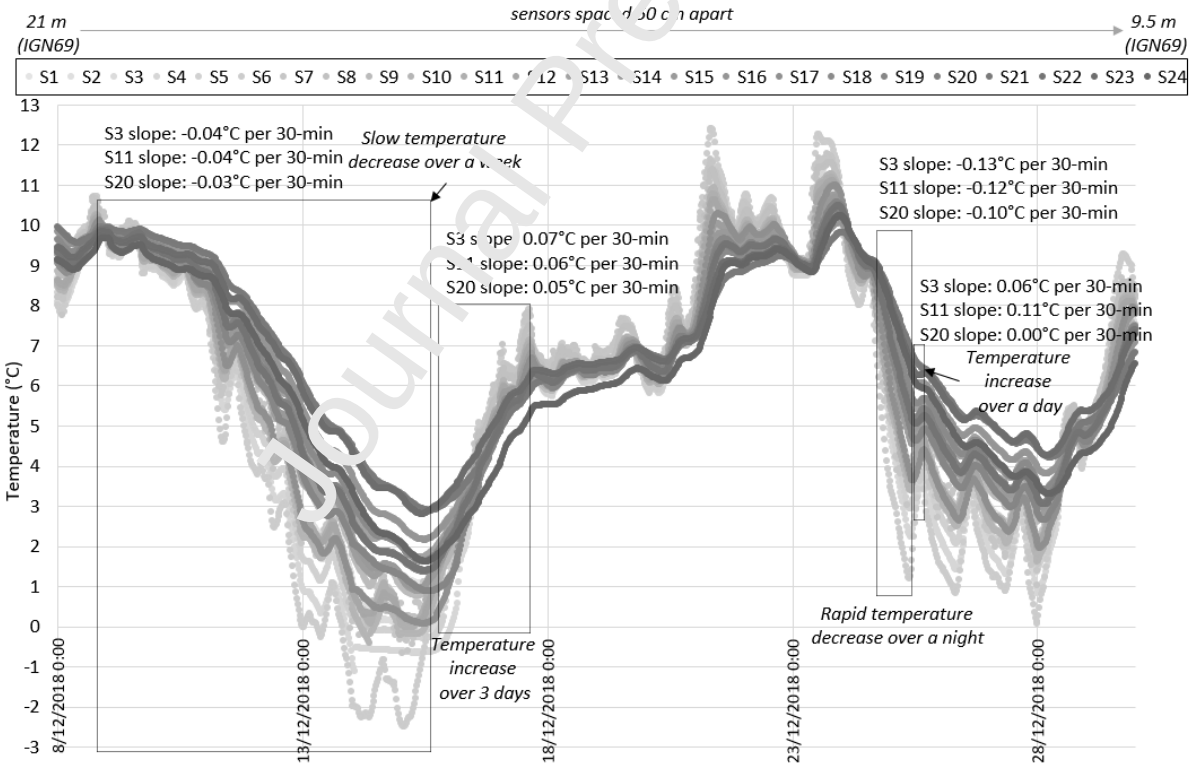

Figure 8: Temperature sensor comparison from 8/12/2018 to 28/12/2018 for the 24 sensors (numbering from the top to the bottom of the cliff face) showing temperature gradients for sensors 3 (S3), 11 (S11) and 20 (S20).

5.4. Preliminary analysis of cliff-top ground motion

Our seismometer measurements show higher levels of energy of displacement in IG and SF bands, compared with the inland reference station, consistent with prior observations associating this response to a swaying motion of the cliff induced by wave action (e.g., Adams et al., 2005; Young et al., 2011). We recorded displacements up to 50 µm, which is similar to prior studies carried out in different environments, covering a range of settings in terms of geology, coastal morphology, wave and weather climates (Adams et al., 2005; Earlie et al., 2015).

Taking a preliminary look at the question of wave-cliff coupling, we consider the transfer function between the swell and the cliff-top ground motion. We focus on a one-month period featuring the change from a regime with larger waves to a regime with smaller waves (Figure 9, upper panel). Significant wave height was derived from the pressure sensor measurements, also using 30 min windows with 83% overlap to compute power spectrum, and using the same frequency bands for SF and IG as defined earlier. We used the ratio of cliff-top ground motion energy to significant wave height as a metric for the wave-cliff transfer function, and we examined this ratio in the IG and SF bands (Figure 9, lower panel). This ratio is small because water waves are on the order of 1 m and ground motion is on the order of 1 µm. The wave-cliff transfer is more efficient (the ratio is about 100 times bigger) in the IG band (black) than in the SF band (red), consistent with prior observations (e.g., Young et al., 2011, 2012; Earlie et al., 2015). We also observe a modulation of the ratio of cliff-top displacement energy to significant wave height, depending on wave height. Energy transfer appears to be more efficient for small waves (last 10 days on the Figure 9) than for large waves (first 20 days on the Figure 9).

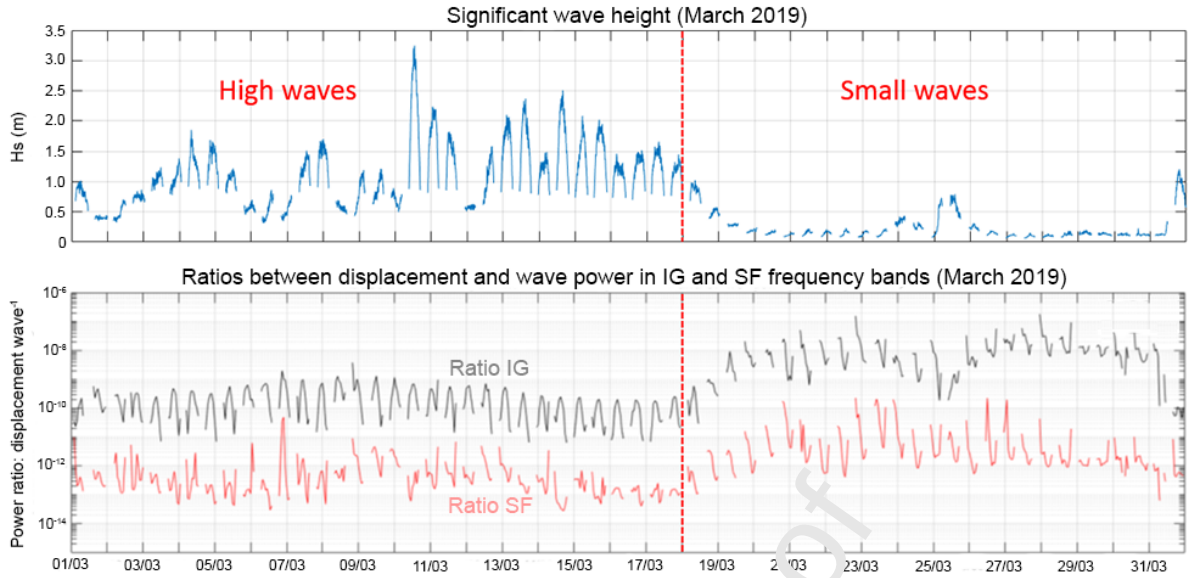

Figure 9: Ratio of cliff-top displacement energy to significant wave height in the IG and SF bands in March 2019

5.5. Displacement on existing fractures

5.5.1. Influence of the tidal amplitude

The time-series of extensometers' data shows a correlation with tidal cycles: significant displacements occur mainly during spring tides (Figure 4). This correlation with the tidal cycles is not systematic. There seems to be a threshold on the tidal amplitude (water level of approximatively 6 m at high tide for the time-series measured with the pressure sensor, corresponding to a tidal level of 9 m above the nautical chart datum or a tidal coefficient of 85) above which significant displacements on extensometers are more frequent and with larger values. In some cases (the spring tides above the threshold in December and January on Figure 4), there is a time lag, larger than 1 day, between the peaks of the envelopes of contraction and extension movements.

5.5.2. Results with both populations of the two-hour periods, with and without displacements

The PCA highlights that the distribution of individuals and variables is scattered. This means that the evolution of existing fractures depends not just on one, but a combination of several

factors. The most significant opposition in the variables tested is with the significant wave height and wind speed (on PC1, synthesizing 34.5% of the total information), and water level and tide coefficient (on PC2, synthesizing 20.6% of the total information).

From the HCA, average of clusters and χ^2 tests, three types of environmental conditions can be identified as being responsible, or not, for the observed displacement on existing fractures (Figure 10):

- Medium significant wave height (0.4 ± 0.2 m), low wind speed (3.0 ± 1.6 m s^{-1}), high water level (4.1 ± 1.4 m), high tide coefficient (87 ± 17), low rainfall (0.0 ± 0.1 mm), medium temperature (5.8 ± 2.3°C) (cluster 1, Figure 10) constitute the preferred situation for displacement over the two-hour periods, both in frequency of occurrence (over-representation of three extensometers and more showing significant displacement, meaning that these conditions are prone to significant displacement of numerous (three or more) extensometers) and in intensity of displacement (over-representation of displacements in absolute value greater than 0.03 mm and under-representation of all extensometers not showing any significant displacement);

- medium significant wave height (0.4 ± 0.2 m), medium wind speed (4.1 ± 2.1 m s^{-1}), low water level (2.0 ± 1.0 m), medium tide coefficient (57 ± 16), medium rainfall (0.1 ± 0.3 mm), medium temperature (6.0 ± 2.4°C) (cluster 2, Figure 10) is the second most favourable cluster for significant displacement with high intensity (over-representation of displacements in absolute value greater than 0.03 mm).

- The least favourable conditions for displacement correspond, surprisingly, to high significant wave height (1.2 ± 0.5 m), high wind speed (7.9 ± 2.2 m s^{-1}), high water level (3.6 ± 1.5 m), medium tide coefficient (70 ± 16), high rainfall (0.3 ± 0.8 mm), high temperature (8.4 ± 1.9°C) (cluster 3, Figure 10). But when displacements occur, they are characterised by low frequency of occurrence (over-representation of only one or two extensometer(s) showing significant displacement) and low intensity of displacement (when there is a displacement, it is less than or equal to 0.03 mm in absolute value).

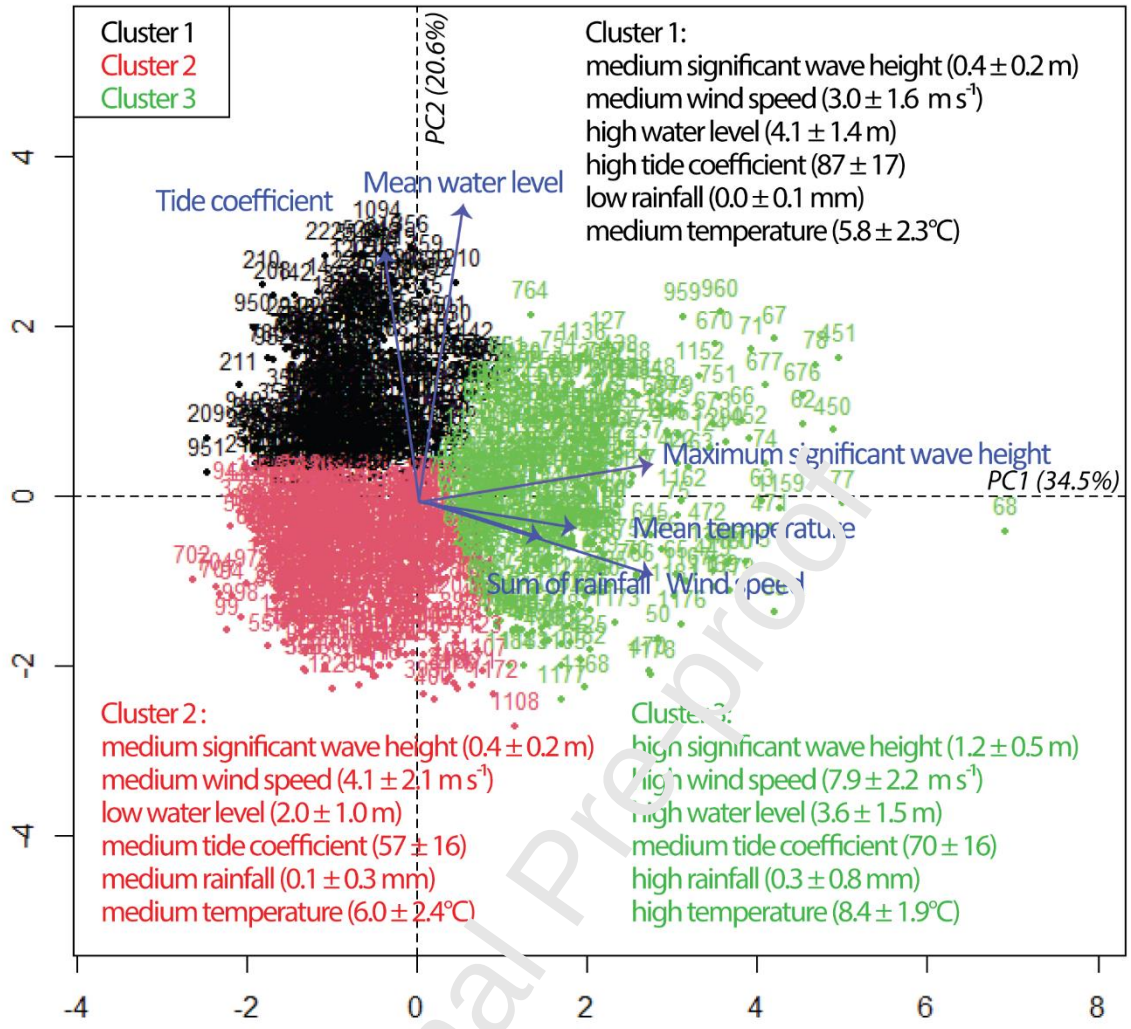

Figure 10: The first two PCA components and the three clusters from HCA on the population of two-hour periods with and without displacements

5.5.3. Results of the population of the two-hour periods only with displacements

The results on the second population (1409 individuals which are considered as displacements) confirm the previous results, going a step further by relating the set of environmental conditions prone to displacement on existing fractures to the direction of displacement recorded on the cliff face. Cluster 1 (medium significant wave height, low wind speed, high water level, high tide coefficient, low rainfall, medium temperature) is the most favourable environmental conditions for extension displacement on existing fractures. Cluster 3 (high significant wave height, high wind speed, high water level, medium tide coefficient,

high rainfall, high temperature) is the most favourable environmental conditions for contraction displacement on existing fractures. We ran a χ^2 test between the types of subaerial and marine conditions and displacement areas on the cliff face (main fracture; secondary fracture; block; flint band; chalk, according to the specific cliff features at the locations where the sensors were deployed) but the differences were not significant.

6. Discussion

Characterising environmental forcing factors and understanding their impact on cliff behaviour and cliff fatigue leading to failure requires continuous monitoring of multiple parameters. The dataset collected in the RICOCHET experiment comprises environmental forcing factors (marine and subaerial), the cliff's mechanical response, and foreshore and cliff morphological evolution, which are essential input data for any modelling of cliff response, including over large spatial and time scales (Limber et al., 2018). Environmental seismology is proving to be a very useful approach for investigating mass movements in various settings (Provost et al., 2018). On coastal cliffs, the observed cliff-top micro-seismic ground motion captures the complex signature of the local, nearshore wave climate, including wave transformation, wave breaking, morphology of the shore platform and cliff foot, providing a measurement of the energy delivery to the cliffs (Vann Jones et al., 2018). Decomposing the wave-cliff transfer function remains a challenge. Here, the cliff-top displacement amplitude values observed by the broadband seismometer, up to 50 µm, are relatively high given the relatively calm conditions. This could be linked to cliff chalk elasticity, which has a static Young's modulus between 3000 and 16000 MPa for dry chalk, and between 740 and 4500 MPa for saturated chalk (Senfaute et al., 2005). Our preliminary observation on the dependence of the ratio of cliff-top displacement energy to significant wave height confirms the strong modulation of the transfer function by the wave climate.

Our results highlight that thermal amplitude is higher at the cliff top than at the cliff foot. Thermal variations may increase fatigue and fracturing of the chalk material, especially with the north-orientation of the cliff face. Indeed, studies have demonstrated that, in humid

temperate climate (Aldred et al., 2016) and mid-latitude desert (McFadden et al., 2005; Eppes et al., 2015, 2010), cracks are preferentially observed in rock walls with northeast orientations. Insolation-related cracking is the main hypothesis, helped by other weathering processes at play (Aldred et al., 2016). A weathering mechanism that may be efficacious is the freeze/thaw cycles in the study site as they occur in a moisture-availability environment (Letavernier and Ozouf, 1987; Prick, 1995). Frost weathering leads to two processes: volumetric expansion and ice segregation (Matsuoka and Murton, 2008). As mentioned in Dewez et al. (2015), in Normandy, temperatures below 0°C (for fresh water) and below -2.5°C (for seawater) contract the rock while pore water freezes and dilates, leading to stress changes. These multidirectional strains accumulate and give rise to the breaking of pore walls and the appearance of micro-crack networks in the rock matrix. Fracturing can occur quickly in intact chalk: Robinson and Jerwood (1987), in laboratory experiments observed erosion in 14 cycles and Murton et al. (2006) confirmed these results of macro-fracturing observations with 10 to 20 simulated successive freeze/thaw cycles. Given our observations on thermal variations, rock falls caused by freeze/thaw cycles would then occur preferentially at the top of the cliff face (Figure 2b, from the cliff edge, around temperature sensor S1 (21 m IGN69) to around S11 (16 m IGN69)). However, the degree of weathering that the chalk undergoes is much more advanced at the cliff foot than elsewhere along the cliff face, which is most likely due to saturation of the chalk at and below the cliff foot, as shown in the geophysical data, and to the addition of marine action at this location. This is consistent with Aldred et al. (2016), who observed that on different field sites in humid temperate climates, the moisture-availability can determine cracking rates. We suggest that this enhanced weathering at the cliff foot, which results from a combination of chemical actions from sea spray (under conditions of high tide and large waves) and groundwater circulation, leads to recurrent failures at this location (rockfalls and flakes) (Figure 11).

Figure 11: Rock falls and flakes observed in Sainte-Marguerite-sur-Mer (05/07/2018)

The presence of groundwater table could also explain the decreasing thermal inertia as a function of cliff height along the outcrop. Water infiltration in rock masses can generate thermal anomalies that are viewable with an infrared camera (Frodella et al., 2017). However, following our six thermal surveys carried out by infrared camera, no thermal anomalies were observed at the cliff foot.

The displacements on the cliff face show a control by the tidal amplitude, with a threshold response. It is as if the tide induced, cyclic cliff face deformation triggered fracture displacement only above a certain threshold on the tidal amplitude. Our multi-parameter monitoring shows that the displacements on existing fractures on the cliff face are multifactorial and complex. Beyond the observed correlation with the tidal amplitude, bivariate and multivariate statistical analysis methods used to identify the conditions most prone to displacements on the cliff face considering a population of two-hour period individuals provide complementary insights. While high significant wave heights, high wind speed, high rainfall are generally considered to be conducive to intense and numerous displacements, here such conditions were the least favourable to displacements. Although it may be due to the absence of severe meteorological and marine conditions, this result is surprising. The displacements measured by the extensometers are very local, and likely with

delays, cascade effects, or combinations of processes and/or hysteresis phenomena. To make the best use of the extensometer data, it would be necessary to detect and then analyse the periods in which the majority of the eight extensometers record simultaneous displacements. To this end, continuous recordings would be needed to identify events of fracture movement, instead of displacement values integrated over 30 min. It will be interesting to continue the analysis of the displacements recorded by the extensometers over the entire 13 months of monitoring which includes periods with more energetic conditions. One of the other perspectives is to compare this dataset with others, including the one previously mentioned and that was acquired in Brittany, with equivalent instruments (Letortu et al., 2017; Laute et al., 2018).

7. Conclusions

For 13 months (from November 2018 to January 2020), continuous, multi-parameter monitoring was set up at the chalk cliff site of Sainte-Marguerite-sur-Mer (Normandy, France) to better understand factors and processes leading to cliff fatigue and cliff failure. This ambitious instrumentation with nine different sensor types was presented in this paper along with the initial results on the structural properties of the chalk massif, and the preliminary results (over the November 2018 to March 2019 period, which turned out to be a very mild and calm winter) of the main subsurface behaviour on the cliff face, cliff-top ground motion and evolution of existing cliff fractures. The geophysical site characterisation shows a two-layer cliff structure: the first 20 m are relatively dry, whereas from the cliff foot and extending at least 20 m beneath, the chalk is saturated with highly conductive fluids (mixing of seawater and inland groundwater). Thermal inertia decreases with the cliff height along the outcrop subsurface. Observations of the cliff-top displacement on this chalk cliff are consistent with previous studies on different types of rocky cliffs. The measured displacement amplitude, up to 50 µm, is rather high considering the relatively calm conditions experienced. This is likely to be related to the elasticity of the chalk material. We also observed that the displacement on existing fractures is partly controlled by the tidal amplitude. Statistical analyses over the

two-hour periods highlight other controls. For the study period, medium significant wave height, low wind speed, high water level, high tide coefficient, low rainfall, medium temperature provided the optimal conditions for high intensity and high frequency of occurrence of displacements, preferentially in extension direction. The research perspectives on this systemic dataset are exciting. Examining fatigue and failure thresholds (leading to rock falls), taking into account cliff structure (lithology, stratigraphy, tectonics), and unravelling the contributions to cliff fracturing from marine and subaerial forcing factors, are contemporary and future challenges our dataset will help to address. In addition, similar multi-parameter monitoring studies on other sites in different coastal cliff environments around the world will enable comparisons so as to identify site-dependent responses and more universal patterns, and to understand how processes controlling cliff fatigue combine in time and space to trigger erosion.

Acknowledgements

This work was supported by the ANR project “RICOCHET: multi-risk assessment on coastal territory in a global change context” funded by the French National Research Agency [ANR-16-CE03-0008]. It was also supported by ISblue project, Interdisciplinary graduate school for the blue planet (ANR-17-EURE-0015) and co-funded by a grant from the French government under the program "Investissements d'Avenir”. We extend our sincerest thanks to M. Ferchal, mayor of Sainte-Marguerite-sur-Mer, L. Voisin and L. Capron for allowing us to use their plot to deploy the instrumentation, and A. Saab and A. Sallent for their precious help on the ground. We would also like to thank the trainees S. Caron and Y. Gratacap who worked with us on this project, and the reviewers for their detailed reading of the manuscript and their helpful comments.

References

Adams, P.N., Anderson, R.S., Revenaugh, J., 2002. Microseismic measurement of wave-energy delivery to a rocky coast. Geology 30, 895–898. https://doi.org/10.1130/0091-7613(2002)030<0895:MMOWED>2.0.CO;2

Adams, P.N., Storlazzi, C.D., Anderson, R.S., 2005. Nearshore wave-induced cyclical flexing of sea cliffs. J. Geophys. Res. Earth Surf. 110. https://doi.org/10.1029/2004JF000217

Aldred, J., Eppes, M.C., Aquino, K., Deal, R., Garbini, J., Swami, S., Tuttle, A., Xanthos, G., 2016. The influence of solar-induced thermal stresses on the mechanical weathering of rocks in humid mid-latitudes. Earth Surf. Process. Landf. 41, 603–614. https://doi.org/10.1002/esp.3849

André, M.-F., 1997. Holocene Rockwall Retreat in Svalbard: A Triple-Rate Evolution. Earth Surf. Process. Landf. 22, 423–440. https://doi.org/10.1002/(SICI)1096-9837(199705)22:5<423::AID-ESP706>3.0.CO;2-3

Augris, C., Clabaut, P., Costa, S., Gourmelon, F., Latteux, B., 2004. Evolution morpho-sédimentaire du domaine littoral et marin de la Seine-Maritime, Ifremer. ed. Paris.

Balk, D., Montgomery, M.R., McGranahan, G., Kim, D., Mara, V., Todd, M., Buettner, T., Dorélien, A., 2009. Mapping Urban Settlements and the Risks of Climate Change in Africa, Asia and South America, in: Population Dynamics and Climate Change, United Nations Population Fund. pp. 80–103.

Bernatchez, P., Boucher-Brossard, G., Corriveau, M., Caulet, C., Barnett, R.L., 2021. Long-Term Evolution and Monitoring at High Temporal Resolution of a Rapidly Retreating Cliff in a Cold Temperate Climate Affected by Cryogenic Processes, North Shore of the St. Lawrence Gulf, Quebec (Canada). J. Mar. Sci. Eng. 9, 1418.

Bernatchez, P., Jolivet, Y., Corriveau, M., 2011. Development of an automated method for continuous detection and quantification of cliff erosion events. Earth Surf. Process. Landf. 36, 347–362. https://doi.org/10.1002/esp.2045

Bertin, X., de Bakker, A., Van Dongeren, A., Coco, G., Andre, G., Ardhuin, F., Bonneton, P., Bouchette, F., Castelle, B., Crawford, W.C., 2018. Infragravity waves: From driving mechanisms to impacts. Earth-Sci. Rev. 177, 774–799.

Bignot, G., 1962. Etude sédimentologique et micropaléontologique de l'Eocène du Cap d'Ailly (près de Dieppe-Seine-Maritime) (PhD Thesis). Paris.

Brooks, S.M., Spencer, T., Boreham, S., 2012. Deriving mechanisms and thresholds for cliff retreat in soft-rock cliffs under changing climates: Rapidly retreating cliffs of the Suffolk coast, UK. Geomorphology 153–154, 48–60. https://doi.org/10.1016/j.geomorph.2012.02.007

Carter, C.H., Guy, D.E., 1988. Coastal erosion: processes, timing and magnitudes at the bluff toe. Mar. Geol. 84, 1–17.

Collins, B.D., Stock, G.M., 2016. Rockfall triggering by cyclic thermal stressing of exfoliation fractures. Nat. Geosci. 9, 395–400. https://doi.org/10.1038/ngeo2686

Costa, S., 1997. Dynamique littorale et risques naturels : L'impact des aménagements, des variations du niveau marin et des modifications climatiques entre la baie de Seine et la baie de Somme (Haute-Normandie, Picardie; France) (PhD Thesis). Paris 1.

Costa, S., Delahaye, D., Freiré-Diaz, S., Di Nocera, L., Davidson, R., Plessis, E., 2004. Quantification of the Normandy and Picardy chalk cliff retreat by photogrammetric analysis. Geol. Soc. Lond. Eng. Geol. Spec. Publ. 20, 139–148.

Costa, S., Lageat, Y., Hénaff, A., 2006a. The gravel beaches of north-west France and their contribution to the dynamic of the coastal cliff-shore platform system. Z. Geomorphol. 144, 199–214.

Costa, S., Laignel, B., Hauchard, E., Delahaye, D., 2006b. Facteurs de répartition des entonnoirs de dissolution dans les craies du littoral du Nord-Ouest du Bassin de Paris. Z. Geomorphol. 50, 95–116. https://doi.org/10.1127/zfg/50/2006/95

Costa, S., Maquaire, O., Letortu, P., Thirard, G., Compain, V., Roulland, T., Medjkane, M., Davidson, R., Graff, K., Lissak, C., Delacourt, C., Duguet, T., Fauchard, C., Antoine, R., 2019. Sedimentary Coastal Cliffs of Normandy: Modalities and Quantification of Retreat. J. Coast. Res. 88, 46–60. https://doi.org/10.2112/SI88-005.1

Dewez, T.J.B., Regard, V., Duperret, A., Lasseur, E., 2015. Shore platform lowering due to frost shattering during the 2009 winter at Mesnil Val, English channel coast, NW France. Earth Surf. Process. Landf. 40, 1688–1700.

Dickson, M.E., Pentney, R., 2012. Micro-seismic measurements of cliff motion under wave impact and implications for the development of near-horizontal shore platforms. Geomorphology 151–152, 27–38. https://doi.org/10.1016/j.geomorph.2012.01.006

Dornbusch, U., Robinson, D.A., Williams, R.B.G., Moses, C.A., 2007. Chalk shore platform erosion in the vicinity of sea defence structures and the impact of construction methods. Coast. Eng. 54, 801–810. https://doi.org/10.1016/j.coastaleng.2007.05.012

Duperret, A., Genter, A., Martinez, A., Mortimore, R.N., 2004. Coastal chalk cliff instability in NW France: role of lithology, fracture pattern and rainfall, in: Coastal Chalk Cliff Instability, Geological Society Engineering Geology Special Publication. Mortimore R.N. and Duperret A., London, pp. 33–55.

Duperret, A., Genter, A., Mortimore, R.N., Delacourt, B., De Pomerai, M.R., 2002. Coastal rock cliff erosion by collapse at Puys, France: The role of impervious marl seams within chalk of NW Europe. J. Coast. Res. 18, 52–61.

Earlie, C.S., Young, A.P., Masselink, G., Russell, P.E., 2015. Coastal cliff ground motions and response to extreme storm waves. Geophys. Res. Lett. 42, 847–854. https://doi.org/10.1002/2014GL062534

Eppes, M.C., McFadden, L.D., Wegmann, K.W., Scuderi, L.A., 2010. Cracks in desert pavement rocks: Further insights into mechanical weathering by directional insolation. Geomorphology 123, 97–108. https://doi.org/10.1016/j.geomorph.2010.07.003

Eppes, M.-C., Willis, A., Molaro, J., Abernathy, S., Zhou, B., 2015. Cracks in Martian boulders exhibit preferred orientations that point to solar-induced thermal stress. Nat. Commun. 6, 6712. https://doi.org/10.1038/ncomms7712

Evrard, H., Sinelle, C., 1987. La stabilité des falaises du Pays de Caux (Normandie), in: Actes Du Colloque “Mer et Littoral. Couple à Risque”, La Documentation Française, Paris. pp. 84–91.

Fauchard, C., Antoine, R., Bretar, F., Lacogne, J., Fargier, Y., Maisonnave, C., Guilbert, V., Marjerie, P., Thérain, P.-F., Dupont, J.-P., Pierrot-Deseilligny, M., 2013. Assessment of an ancient bridge combining geophysical and advanced photogrammetric methods: Application to the Pont De Coq, France. J. Appl. Geophys. 98, 100–112. https://doi.org/10.1016/j.jappgeo.2013.08.009

Guilcher, A., 1954. Morphologie littorale et sous-marine. Presses universitaires de France.

Hutchinson, J.N., 1969. A Reconsideration of the Coastal Landslides at Folkestone Warren, Kent. Géotechnique 19, 6–38. https://doi.org/10.1680/geot.1969.19.1.6

Ilinca, V., 2009. Rockfall hazard assessment. Case study: Lotru Valley and Olt Gorge. Rev. Geomorfol. 11, 101–108.

IPCC, 2022. IPCC 2022: Summary for Policymakers, in: Climate Change 2022: Impacts, Adaptation and Vulnerability. Cambridge University Press, p. 35.

IPCC, 2021. IPCC, 2021: Summary for Policymakers, in: Climate Change 2021: The Physical Science Basis. Working Group I Contribution of Working Group I to the Sixth Assessment Report of the Intergovernmental Panel on Climate Change. p. 31.

Kennedy, D.M., Jones, E.C.V., Dickson, M.E., Rosser, N.J., 2018. Wind Waves and Cliff Shaking on Macrotidal Shore Platforms: A Case-study from North Yorkshire, U.K. J. Coast. Res. 436–440. https://doi.org/10.2112/SI85-088.1

Kennedy, D.M., Stephenson, W.J., Naylor, L.A., 2014. Rock coast geomorphology: A global synthesis, Geological Society. ed. Kennedy D.M., Stephenson W.J. and Naylor L.A., London.

Lageat, Y., Hénaff, A., Costa, S., 2006. The retreat of the chalk cliffs of the Pays de Caux (France): erosion processes and patterns. Z. Für Geomorphol. 144, 183–197.

Laignel, B., 1997. Les altérites à silex de l'ouest du Bassin de Paris: caractérisation lithologique, genèse et utilisation potentielle comme granulats (PhD Thesis). Rouen.

Laute, K., Letortu, P., Le Dantec, N., Hibert, C., Augereau, E., Provost, F., Malet, J.-P., 2018. Driving factors of hard rock cliff erosion in Brittany, France. Geophys. Res. Abstr. 1. https://meetingorganizer.copernicus.org/EGU2018/EGU2018-9029-1.pdf

Lawler, D.M., 2005. The importance of high-resolution monitoring in erosion and deposition dynamics studies: examples from estuarine and fluvial systems. Geomorphology 64, 1–23. https://doi.org/10.1016/j.geomorph.2004.04.005

Lee, E.M., 2008. Coastal cliff behaviour: Observations on the relationship between beach levels and recession rates. Geomorphology 101, 558–571. https://doi.org/10.1016/j.geomorph.2008.02.010

Letavernier, G., Ozouf, J.C., 1987. Résultats des recherches récentes sur la gélifraction des calcaires. Inter-Nord 53–63.

Letortu, P., Costa, S., Bensaid, A., Cador, J.-M., Quénol, H., 2014a. Vitesses et modalités de recul des falaises crayeuses de Haute-Normandie (France): méthodologie et variabilité du recul. Geomorphol. Relief Process. Environ. 20, 133–144. https://doi.org/10.4000/geomorphologie.10872

Letortu, P., Costa, S., Bonnet, E., 2014b. Spatial analysis of coastal chalk cliff falls in upper Normandy (France). From Veules-les-Roses to Le Treport (2002-2009). Rev. Int. Géomat. 24, 335–354. https://doi.org/10.3166/rig.24.335-354

Letortu, P., Costa, S., Cador, J.-M., Cornaud, C., Cantat, O., 2015a. Statistical and empirical analyses of the triggers of coastal chalk cliff failure. Earth Surf. Process. Landf. 40, 1371–1386. https://doi.org/10.1002/esp.3741

Letortu, P., Costa, S., Maquaire, O., Davidson, R., 2019. Marine and subaerial controls of coastal chalk cliff erosion in Normandy (France) based on a 7-year laser scanner monitoring. Geomorphology 335, 76–91. https://doi.org/10.1016/j.geomorph.2019.03.005

Letortu, P., Costa, S., Maquaire, O., Delacourt, C., Augereau, E., Davidson, R., Suanez, S., Nabucet, J., 2015b. Retreat rates, modalities and agents responsible for erosion along the coastal chalk cliffs of Upper Normandy: The contribution of terrestrial laser scanning. Geomorphology 245, 3–14. https://doi.org/10.1016/j.geomorph.2015.05.007

Letortu, P., Laute, K., Le Dantec, N., Augereau, E., Ammann, J., Prunier, C., Hénaff, A., David, L., Maulpoix, A., Cuq, V., 2017. Impacts des vagues et de la circulation d'eau sur la microfracturation des falaises rocheuses: mise en place d'un suivi multiparamètre en Bretagne. Collect. EDYTEM Cah. Géographie 251–256.

Lim, M., Rosser, N.J., Allison, R.J., Petley, D.N., 2010. Erosional processes in the hard rock coastal cliffs at Staithes, North Yorkshire. Geomorphology 114, 12–21. https://doi.org/10.1016/j.geomorph.2009.02.011

Lim, M., Rosser, N.J., Petley, D.N., Keen, M., 2011. Quantifying the controls and influence of tide and wave impacts on coastal rock cliff erosion. J. Coast. Res. 27, 46–56. https://doi.org/10.2112/JCOASTRES-D-09-00061.

Limber, P.W., Barnard, P.L., Vitousek, S., Erikson, L.H., 2018. A model ensemble for projecting multidecadal coastal cliff retreat during the 21st century. J. Geophys. Res. Earth Surf. 123, 1566–1589. https://doi.org/10.1029/2017JF004401

Loke, D.M.H., 2004. Tutorial : 2-D and 3-D electrical imaging surveys. https://sites.ualberta.ca/~unsworth/UA-classes/223/loke_course_notes.pdf

Loke, M.H., 2002. RES2DINV, Ver. 3.50, Rapid 2-D Resistivity and IP Inversion Using the Least Square Method. Geotomo Software, Penang.

Mainieri, R., Corona, C., Chanteire, J., Eckert, N., Lopez-Saez, J., Stoffel, M., Bourrier, F., 2020. Dating of rockfall damage in trees yields insights into meteorological triggers of process activity in the French Alps. Earth Surf. Process. Landf. 45, 2235–2250. https://doi.org/10.1002/esp.4876

Matsuoka, N., Sakai, H., 1999. Rockfall activity from an alpine cliff during thawing periods. Geomorphology 28, 309–328. https://doi.org/10.1016/S0169-555X(98)00116-0

McFadden, L.D., Eppes, M.C., Gillespie, A.R., Hallet, B., 2005. Physical weathering in arid landscapes due to diurnal variation in the direction of solar heating. GSA Bull. 117, 161–173. https://doi.org/10.1130/B25508.1

Météo-France, 2019. Fiche climatologique Dieppe (76), statistiques (1981-2010) et records.

Mortimore, R.N., Duperret, A., 2004. Coastal chalk cliff instability. Geological Society of London, London.

Mortimore, R.N., Stone, K.J., Lawrence, J., Duperret, A., 2004. Chalk physical properties and cliff instability, in: Coastal Chalk Cliff Instability, Geological Society Engineering Geology Special Publication. pp. 75–88.

Murton, J.B., Peterson, R., Ozouf, J.-C., 2006. Bedrock fracture by ice segregation in cold regions. Science 314, 1127–1129. https://doi.org/10.1126/science.1132127

Naylor, L.A., Stephenson, W.J., Trenhaile, A.S., 2010. Rock coast geomorphology: Recent advances and future research directions. Geomorphology 114, 3–11. https://doi.org/10.1016/j.geomorph.2009.02.004

Norman, E.C., Rosser, N.J., Brain, M.J., Petley, D.N., Lim, M., 2013. Coastal cliff-top ground motions as proxies for environmental processes. J. Geophys. Res. Oceans 118, 6807–6823. https://doi.org/10.1002/2013JC008963

Pierre, G., Lahousse, P., 2006. The role of groundwater in cliff instability: An example at Cape Blanc-Nez (Pas-de-Calais, France). Earth Surf. Process. Landf. 31, 31–45. https://doi.org/10.1002/esp.1219

Pomerol, B., Bailey, H.W., Mongenardini, C., Mortimore, R.N., 1987. Lithostratigraphy and biostratigraphy of the Lewes and Seaford chalks: A link across the Anglo-Paris Basin at the Turonian-Senonian boundary. Cretac. Res. 8, 289–304.

Poppeliers, C., Mallinson, D., 2015. High-frequency seismic noise generated from breaking shallow water ocean waves and the link to time-variable sea states. Geophys. Res. Lett. 42, 8563–8569. https://doi.org/10.1002/2015GL066126

Prêcheur, C., 1960. Le littoral de la Manche, de Sainte-Adresse à Ault: étude morphologique. Poitiers: SFIL.

Prémaillon, M., Regard, V., Dewez, T.J., Auda, Y., 2018. GlobR2C2 (Global Recession Rates of Coastal Cliffs): a global relational database to investigate coastal rocky cliff erosion rate variations. Earth Surf. Dyn. 6, 651–668. https://doi.org/10.5194/esurf-6-651-2018

Prick, A., 1995. Dilatometrical behaviour of porous calcareous rock samples subjected to freeze-thaw cycles. CATENA, Experimental Geomorphology and Landscape Ecosystem Changes 25, 7–20. https://doi.org/10.1016/0341-8162(94)00038-G

Provost, F., Malet, J.-P., Hibert, C., Abanco Martínez de Arenzana, C., Hurlimann Ziegler, M., 2018. Towards a standard typology of endogenous landslide seismic sources. Earth Surf. Dyn. 6, 1059–1088. https://doi.org/10.5194/esurf-6-1059-2018

Rapp, A., 1960. Recent Development of Mountain Slopes in Kärkevagge and Surroundings, Northern Scandinavia. Geogr. Ann. 42, 65–200. https://doi.org/10.1080/20014422.1960.11880942

Reid, M.E., Nielsen, H.P., Dreiss, S.J., 1988. Hydrologic Factors Triggering a Shallow Hillslope Failure. Environ. Eng. Geosci. xxv, 343–361. https://doi.org/10.2113/gseegeosci.xxv.3.349

Robinson, D., Jerwood, L., 1987. Sub-aerial weathering of chalk shore platforms during harsh winters in Southeast England. Mar. Geol. 77, 1–14.

Robinson, L.A., 1977. Marine erosive processes at the cliff foot. Mar. Geol. 23, 257–271. https://doi.org/10.1016/0025-3227(77)90022-6

Rodgers, P.W., 1968. The response of the horizontal pendulum seismometer to Rayleigh and Love waves, tilt, and free oscillations of the Earth. Bull. Seismol. Soc. Am. 58, 1385–1406.

Saporta, G., 2006. Probabilités, analyse des données et statistique. Editions Technip.

Senfaute, G., Amitrano, D., Lenhard, F., Morel, J., 2005. Étude en laboratoire par méthodes acoustique : de l'endommagement des roches de craie et corrélation avec des résultats in situ. Rev. Fr. Géotechnique 9–18. https://doi.org/10.1051/geotech/2005110009

Sunamura, T., 1977. A relationship between wave-induced cliff erosion and erosive force of waves. J. Geol. 85, 613–618.

Teisson, C., 1986. Houle de projet et durées de tempêtes sur le site de Penly - Analyse de la houle naturelle (LNH HE-42/86 No. 2). LNH.

Thompson, C.F., Young, A.P., Dickson, M.E., 2019. Wave impacts on coastal cliffs: Do bigger waves drive greater ground motion? Earth Surf. Process. Landf. 44, 2849–2860. https://doi.org/10.1002/esp.4712

Vann Jones, E.C., Rosser, N.J., Brain, M.J., 2018. Alongshore variability in wave energy transfer to coastal cliffs. Geomorphology 322, 1–14. https://doi.org/10.1016/j.geomorph.2018.08.019

Vann Jones (née Norman), E.C., Rosser, N.J., Brain, M.J., Petley, D.N., 2015. Quantifying the environmental controls on erosion of a hard rock cliff. Mar. Geol. 363, 230–242. https://doi.org/10.1016/j.margeo.2014.12.008

Varnes, D.J., 1978. Slope movement types and processes, in: Landslides: Analysis and Control. Washington, pp. 11–33.

Viles, H.A., 2013. Linking weathering and rock slope instability: non-linear perspectives. Earth Surf. Process. Landf. 38, 62–70. https://doi.org/10.1002/esp.3294

Wieczorek, G.F., Jäger, S., 1996. Triggering mechanisms and depositional rates of postglacial slope-movement processes in the Yosemite Valley, California. Geomorphology 15, 17–31. https://doi.org/10.1016/0169-555X(95)00112-I

WSDOT, 2021. Geotechnical Design Manual. Washington State Department of Transportation.

Young, A.P., Adams, P.N., O'Reilly, W.C., Flick, R.E., Guza, R.T., 2011. Coastal cliff ground motions from local ocean swell and infragravity waves in southern California. J. Geophys. Res. Oceans 116. https://doi.org/10.1029/2011JC007175

Young, A.P., Guza, R.T., Adams, P.N., O'Reilly, W.C., Flick, R.E., 2012. Cross-shore decay of cliff top ground motions driven by local ocean swell and infragravity waves. J. Geophys. Res. Oceans 117. https://doi.org/10.1029/2012JC007908

Young, A.P., Guza, R.T., Dickson, M.E., O'Reilly, W.C., Flick, R.E., 2013. Ground motions on rocky, cliffed, and sandy shorelines generated by ocean waves. J. Geophys. Res. 118, 6590–6602. https://doi.org/10.1002/2013JC008883

Young, A.P., Guza, R.T., Matsumoto, H., Merrifield, M.A., O'Reilly, W.C., Swirad, Z.M., 2021. Three years of weekly observations of coastal cliff erosion by waves and rainfall. Geomorphology 375, 107545. https://doi.org/10.1016/j.geomorph.2020.107545

Young, A.P., Guza, R.T., O'Reilly, W.C., Burvingt, O., Flick, R.E., 2016. Observations of coastal cliff base waves, sand levels, and cliff top shaking. Earth Surf. Process. Landf. 41, 1564–1573. https://doi.org/10.1002/esp.3928

Zielonka, A., Wrońska-Wałach, D., 2019. Can we distinguish meteorological conditions associated with rockfall activity using dendrochronological analysis? - An example from the Tatra Mountains (Southern Poland). Sci. Total Environ. 662, 422–433. https://doi.org/10.1016/j.scitotenv.2019.01.243

Declaration of interests

☒ The authors declare that they have no known competing financial interests or personal relationships that could have appeared to influence the work reported in this paper.

☐The authors declare the following financial interests/personal relationships which may be considered as potential competing interests:

Highlights:

- A monitoring system was implemented along the chalk cliff coast in Sainte-Marguerite-sur-Mer (Normandy) to better understand the forcing agents and processes that lead to cliff fatigue and failure.
- Between November 2018 and January 2020, 9 types of sensors simultaneously recorded cliff mechanical response, marine forcing agents and subaerial agents.
- The magnitude of cliff-top displacement on this coastal chalk cliff is consistent with prior studies conducted in different settings, showing rather high displacement amplitudes (up to 50 µm despite relatively calm conditions) likely to be related to chalk elasticity.
- In the absence of intense meteorological and marine conditions, the displacement on existing fractures on the cliff face is partly controlled by the tidal amplitude but the phenomenon is multifactorial.